scientific reports

Check for updates

OPEN

Biosynthesis and activity of Zn-MnO nanocomposite in vitro with molecular docking studies against multidrug resistance bacteria and inflammatory activators

Samy Selim[1]✉, Tarek M. Abdelghany[2]✉, Mohammed S. Almuhayawi[3], Mohammed K. Nagshabandi[4], Muyassar K. Tarabulsi[4], Mohammed Yagoub Mohammed Elamir[1], Asmaa A. Alharbi[5] & Soad K. Al Jaouni[6]✉

This study investigated the green synthesis of Zn-MnO nanocomposites via the fungus *Penicillium rubens*. Herein, the synthesized Zn-MnO nanocomposites were confirmed by UV-spectrophotometry with a top peak (370 nm). Transmission electron microscopy confirmed irregular particles with a spherical-like shape ranging from 25.13 to 36.21 nm. Numerous functional groups were detected on the surface of Zn-MnO nanocomposite via Fourier-transform infrared spectroscopy. X-Ray diffraction assay appeared that the synthesized Zn-MnO nanocomposites contained two different components, MnO (JCPDS 81-2261) and ZnO (JCPDS 36-1451), while energy dispersive X-ray spectra confirmed the occurrence of manganese, zinc, oxygen, and carbon in Zn-MnO nanocomposites. Zn-MnO nanocomposites demonstrated excellent suppress effect versus the growth of various bacteria namely *Staphylococcus aureus*, Methicillin-resistant *S. aureus* (MRSA), *Salmonella typhi*, and *Klebsiella pneumoniae* via agar well diffusion assays with inhibition areas of 36 ± 0.1, 25 ± 0.1, 27 ± 0.2, and 23 ± 0.2 mm, correspondingly. Alterations in the ultrastructure of the treated *K. pneumoniae* by Zn-MnO nanocomposite were recorded. Both the values of minimum inhibitory concentration (MIC) and minimum bactericidal concentration of Zn-MnO nanocomposite extended from 15.62 to 125 µg/mL employing the examined bacteria. The antibiofilm activity of Zn-MnO nanocomposites was 82.07, 75.43, 43.65, and 41.35% at 25% MIC, and 96.54, 93.0, 94.53, and 91.11% at 75% MIC against *S. aureus*, MRSA, *K. pneumoniae*, and *S. typhi*, respectively. At 25 to 75% MIC, Zn-MnO nanocomposites exhibited antihemolytic activity with the maximum activity of 96.3% at 75% MIC in the presence of MRSA. Extensive molecular docking studies were performed to identify the optimal location for manganese oxide and zinc oxide nanoclusters binding to MRSA. MnO-NPs and ZnO-NPs demonstrated inhibitory activity against the crystal structure of putative minohydrolase (PDB ID: 4EWT), methicillin acyl-penicillin binding protein 2a structure (PDB ID: 1MWU) and K2U bound crystal structure of class II peptide deformylase from MRSA (PDB ID: 6JFQ). The minimum binding energy was utilized to estimate the receptor's binding site with NPs, providing additional understanding of the ways of action. Anti-inflammatory activity of Zn-MnO nanocomposites via cyclooxygenase-1 and cyclooxygenase-2 enzymes inhibition was documented with IC_{50} doses of 20.81 ± 0.68 µg/mL and 35.87 ± 1.35 µg/mL, respectively. Based on these outcomes, it was concluded that Zn-MnO nanocomposites could be useful agents for the management of multidrug resistant bacterial pathogens and inflammation.

Keywords Cyclooxygenase, Zn-MnO, nanocomposite, Molecular docking, Bacterial pathogens

[1]Department of Clinical Laboratory Sciences, College of Applied Medical Sciences, Jouf University, Sakaka 72388, Kingdom of Saudi Arabia. [2]Botany and Microbiology Department, Faculty of Science, Al-Azhar University, Cairo 11725, Egypt. [3]Department of Clinical Microbiology and Immunology, Faculty of Medicine, King Abdulaziz University, Jeddah 21589, Kingdom of Saudi Arabia. [4]Department of Basic Medical Sciences, College of Medicine, University of Jeddah, Jeddah, Kingdom of Saudi Arabia. [5]Department of Biology, College of Science, Jazan University, Jazan, Kingdom of Saudi Arabia. [6]Department of Hematology/Oncology, Yousef Abdulatif Jameel Scientific Chair of

Prophetic Medicine Application, Faculty of Medicine, King Abdulaziz University, Jeddah 21589, Kingdom of Saudi Arabia. ✉email: sabdulsalam@ju.edu.sa; tabdelghany.201@azhar.edu.eg; saljaouni@kau.edu.sa

In the present decade, science of nano has appeared as a promising tool with a varied array of uses in the mechanical, biological, chemical, food processing, environmental and pharmaceutical industries[1–4]. Through previous studies, numerous approaches for the production of metal-based nanoparticles (NPs) have been described, comprising chemical, physical, and biological. Despite this, research is still ongoing to choose the safest and least expensive methods, and to address the various drawbacks and advantages of each method. Biological methods are preferred over other methods of NPs synthesis for several reasons, including minimal cost and reduced environmental impact, in addition to their utilization of renewable sources. In contrast, physical techniques liberate heat and energy into the atmosphere, while the release of hazardous compounds and toxic products are associated with chemical techniques. Several biological sources can be used for NPs synthesis, including filamentous fungi, bacteria, yeasts, algae, and plants[5,6]. Among these, fungal-mediated synthesis has superior properties and takes advantage of several metabolites that are used as reducers and stabilizers for NPs synthesis[7]. Initially, the field of NPs synthesis focused on the production of one type metal oxide, namely silver (Ag), silicon (Si), zinc (Zn), copper (Cu), Iron (Fe), magnesium (Mg), selenium (Se), nickel (Ni), titanium (Ti), Manganese (Mn), and gold (Au)[8–10], but the area later evolved into the synthesis of two, and sometimes three, different metals as composites[11] due to their stability, alliterative effect, and high activity[12,13]. The activity of formulated dual or triple nanostructures, as well as nancomposites, was greater than that of the individual NPs[14–16].

Several biological activities were attributed to numerous inorganic NPs such as Si, Ag, Au, Fe, Cu, Mg, Zn and Ti[17]. However not all these NPs possess the same bioactivity and safety level, for instance the antibacterial activity of Ag NPs was reported at low concentrations while its high concentration can cause cytotoxic[18]. Also excellent antimicrobial activity was attributed to Au NPs but there are some investigations about its cytotoxicity[19]. In addition, the real applications of Au and Ag NPs are limited due to their high unit costs.

In our study Zn (Bluish-white, solid, point of melting 419.5 °C, density 7.14 g/cm at 25 °C with molecular weight 65.38), and Mn (Steel-gray, solid, melting point 1,244 °C, Density 7.26 g/cm at 20 °C with molecular weight 54.94) in the form nanocomposite were synthesized, characterized, and applied in some biological investigations. The inexpensive cost of Zn attracts the investigators attention for utilization of ZnO NPs in biological functions. Antibacterial and antioxidant properties of Mn_3O_4 are reported. Their properties were enhanced through cooperation with other metals[20]. Enhancement of physiological functions of human was associated with the existence of Mn[21]. The incorporation of ZnO NPs with Mn displayed better biological functions such as antimicrobial and antioxidant activities[22,23].

ZnO NPs and MnO NPs are becoming progressively attractive specific in biological utilization, including nanomedicine, gene transfer, besides pharmaceutical management due to their safety and stability. ZnO NPs possess antibacterial and antifungal properties, so they can apply to inhibit and manage the spread of pathogens[24]. Recently, several methods for producing pertinent MnO NPs, like MnO_2 NPs, Mn_2O_3 NPs, and Mn_3O_4 NPs, have been reported[11,25]. These NPs are potent antibacterial and antioxidant agents since they contain a stable metal oxide with complementary qualities. MnO_2 NPs have also garnered a lot of interest since it is believed that they display limited potential for cytotoxicity compared to other NPs[26]. A range of unique properties, such as nontoxicity, cost-effectiveness, biocompatibility, and thermal and chemical stability, may be present in the nanocomposite that result from the formulation of MnO_2 and ZnO. These properties should be further explored for a range of therapeutic employs, like drug delivery and antimicrobial activity[27]. Dual or triple nanocomposites, on the other hand, have received less attention despite showing great promise in a variety of applications[28]. Moreover, Zn-MnO NPs display a variety of biological activities against pathogenic microorganisms, diabetes, and cancer depending on their stability, concentration, shape and size. EL-Moslamy et al.[15] reported that Zn-MnO NPs synthesized by microorganisms having antimicrobial activity against different bacteria and fungi[16].

Multidrug resistant (MDR) bacteria and their biofilm are usually linked with serious health problems. Abdelraheem et al.[29] reported that linezolid resistant-*Staphylococcus aureus*, vancomycin resistant-*S. aureus* and methicillin resistance-*S. aureus* were significant inhibited by ZnO NPs. The cyclooxygenase (COX) enzyme is activated during inflammation and is essential for prostaglandin synthesis[30]. Prostaglandins are hormone-like molecules that play a variety of roles in the body, such as causing fever, pain, and inflammation[31,32].

Molecular docking (MD) technology is used to evaluate the bioactivity of any discovered compound or any compound developed through its interaction with target proteins. The evaluation of any compound activity is done by calculating the binding affinities those results from the MD interactions, as mentioned in many published scientific papers that focused on natural compounds of plant or microbial origin, as well as NPs that functioned as antimicrobial or anticancer agents[7,33–36]. Therefore, the aim of the present scientific investigation was the synthesis of Zn-MnO nanocomposite via green method and assessing their activities against some multidrug resistance bacteria with MD studies besides its activity as anti-inflammatory activator via cyclooxygenase-1 and cyclooxygenase-2 enzymes inhibition assay.

Therefore, the purpose of the present scientific research was the synthesis of Zn-MnONPs composites via green method and assessing their activities against some multidrug resistance bacteria with MD studies besides its activity as anti-inflammatory activator via cyclooxygenase-1 and cyclooxygenase-2 enzymes inhibition assay.

Materials and methods

Microbial growth

Penicillium rubens (GenBank accession number OM836432.1), marine fungus an endophytic on *Avicennia marina* leaves obtained from Prof. Tarek Mohamed, Al-Azhar University, Egypt, was cultivated in broth of Potato Dextrose for 6 days at 25 °C with shaking (150 rpm). After this period, the developed fungal mycelia

were removed, followed by centrifugation of broth medium at 10,000 rpm for 10 min to removing any debris of mycelia[37]. Via filter (0.2 µm pore size), the collected supernatant was filtered and then used for the synthesis of Zn-MnO nanocomposite.

Biosynthesis of Zn-MnO nanocomposite

In the current experiment, fungal supernatant was assessed for its ability to synthesize Zn-MnO nanocomposites as potent metal oxide tolerance agents. The nanocomposite precursors including Zn $(CH_3COO)_2{\cdot}2H_2O$ and $MnCl_2$ were prepared as 200 mM and 100 mM solutions, respectively, in deionized H_2O, and then equal volumes of each precursor were mixed. The fungal supernatant (200 mL) was adjusted to pH 6 using 5 M NaOH and then applied as a reducatant agent of nanocomposite precursors. The extract was titrated toward precursors mixture pending the color of extract shifted markedly, followed by shaking at 200 rpm and 50 °C for 60 min. Lastly, the diluted extract (20%) (15 mL) was added to the reaction mixture as a capping agent[16]. The produced Zn-MnO nanocomposite was lyophilized in powder form.

Characterizations of Zn-MnO nanocomposite

The shape and size of Zn-MnO nanocomposites were investigated via Transmission electron microscopy (TEM) (Philips CM-200, Japan). The UV–Vis spectroscopy technique was applied to detect the optical possessions of synthesized Zn-MnO nanocomposite. Morphology and elemental analysis of Zn-MnO nanocomposite were determined via Energy dispersive x-ray (EDX) joined with scanning electron microscopy (SEM-JEOL JSM 840 A, China). The Zn-MnO nanocomposite powder's characteristics are examined through X-ray diffraction (XRD) (Shimadzu 7000 Diffractometer) that uses Cu $K\alpha_1$ radiation (k _ 0.15406 nm). With a scan rate of 2°/min and 2° values ranging from 0° to 80°, this XRD pattern was produced at 30 kV and 30 mA. Before being shaped into a pellet, the air-dried powder of Zn-MnO nanocomposites with 0.25–0.50 KBr was thoroughly mixed and ground in a mortar. Then the prepared pellet of Zn-MnO nanocomposite was examined by a Japanese instrument (Shimadzu FTIR-8400 S) FTIR spectra that span the 400–4000 cm^1 range of wavelength. Stability of Zn-MnO nanocomposite was characterized via dynamic light scattering (DLS) model Horiba, SZ-100, Japan. Zn-MnO nanocomposite after dilution, it dispersed via sonication process for 25 min, and then investigated utilizing DLS at 25 °C[16].

Efficacy Zn-MnO nanocomposites against tested bacteria

Some multi-drug resistant human pathogens, comprising methicillin-resistant *Staphylococcus aureus* (ATCC 33591) (MRSA), *S. aureus* (ATCC 6538), *Klebsiella pneumoniae* (ATCC13883), *Salmonella typhi* (ATCC 6539) were employed for estimating the Zn-MnO nanocomposite's antimicrobial susceptibility in vitro. Employing the agar well diffusion technique, the antimicrobial properties of the synthesized Zn-MnO nanocomposites were examined. First, LB broth medium was used to cultivate every human pathogen that was tested. Next, 100 µL of the cell suspension (1 × 106 CFU/mL) for each pathogen was swabbed separately onto LB agar plates. After that, a sterile cork borer (5 mm) was used to drill the wells in each plate. After that, 25 µL of 100 µg/mL of tested Zn-MnO nanocomposite was added to each of these wells independently. DMSO (30 µL/well) and 5 mg/mL of ampicillin were prepared as controls negative and positive, respectively. Following a 2-hour statically incubated period at 4 °C for well-diffusion, the plates were moved to a 48-hour incubator at 37 °C. Following this period, the inhibitory areas that developed were measured in millimeters[14]. Ultrastructure studies were done on one bacterium (*K. pneumoniae*) as a model to evaluate the action mechanism of Zn-MnO nanocomposite for inhibition the bactterial growth. *K. pneumoniae* was treated by 100 µg/mL of Zn-MnO nanocomposite, after the 24 h of growth period, it examine by Transmission electron microscopy (TEM)[38].

Approach of Broth Micro Dilution to estimate MIC and MBC of Zn-MnO nanocomposites

The minimum bactericidal concentration (MIC) of Zn-MnO nanocomposites was detected using the microdilution approach in hygienic plastic plates with round wells holding 0.1 mL of broth. Zn-MnO nanocomposite was prepared in serial dilutions and subsequently distributed into the microdilution trays. The supplying apparatus then fills each of the 96 standard tray wells with 0.1 mL. A saline solution contained 2×10^8 colony-forming units/mL (adjusted to a 0.5 McFarland standard) was used to prepare the microbial inoculum suspension. Within 15 min of the inoculation procedure, the wells were inoculated and allowed to incubate in ambient air incubator for 20 h at 37 °C. The MIC is the lowest concentration of Zn-MnO nanocomposites that, when measured by recording the OD at 600 nm, totally inhibits the development of the tested bacteria in microdilution wells. The microbial culture was diluted to a concentration of 1×10^5 colony-forming units/mL in Mueller Hinton Broth in order to detect the minimum bactericidal concentration (MBC) of Zn-MnO nanocomposite. Zn-MnO nanocomposite is prepared in 96-well microtiter plates in 1:1 dilutions in addition to a stock dilution made 100 times of the detected MIC. Each dilution and tested bacteria were inoculated in equal volumes. In order to demonstrate acceptable bacterial development over the course of the incubation period and media sterility, respectively, tested bacteria were injected in positive as well as negative control wells[39]. To create a baseline dilution of the employed bacteria, an aliquot of the appeared bacteria (positive control) is cultivated. Incubation of the Microtiter plates was then carried out for 48 h at 35 °C. Bacteria development is indicated by turbidity, and the minimum inhibitory concentration (MIC) is the concentration at which no microbial growth is observed. A minimum of two of the more concentrated sample dilutions are plated and calculated to record the viable CFU/ml in order to calculate the MBC. MIC is represented by the dilution. With respect to the MIC dilution, the MBC is the lowest quantity that exhibits a predetermined decline (99.9%) in CFU/mL at what time.

Anti-biofilm activity

In 96-well polystyrene flat bottom plates, the influence of the nanoparticles on the formation of bacterial biofilms was evaluated. 300µL of freshly inoculated Mueller–Hinton Broth (MHB) medium, with a final dose of 10^6 CFU/mL, was added to each well of a microplate. The TSY was then cultivated in the existence of the previously calculated sublethal dosages of Zn-MnO nanocomposites MBC (75, 50, and 25%). As controls, there were wells with medium, wells with only methanol, and wells devoid of any Zn-MnO nanocomposite. For 48 h, plates were incubated at 37 °C. After the incubation time, the supernatant was detached, and sterile distilled H_2O was employed to thoroughly wash the free-floating cells in each well. The bio-film that had formed was stained using aqueous solution of crystal violet (0.1%) for 15 min at 25℃ after the plates were left to air dry for 30 min. Water was used to remove any excess stain following incubation. Following incubation, the plate was cleaned three times with sterile distilled water to get rid of any leftover dye. The dye joined to the cells was eventually solubilized via addition of 250 µL ethyl alcohol (95%) to each well once 15 min of incubation[40]. Next, the absorbance was determined at 570 nm employing a microplate reader.

$$\text{Anti-biofilm activity } \% = \text{ abs control } - -\text{abs Zn} - \text{MnO nanocomposite/abs control} \times 100$$

Hemolysis measurement of Zn-MnO nanocomposite in the existence of tested bacteria

The hemolysin activity of Zn-MnO nanocomposite in sub-MIC of 25%, 50%, and 75% treated with the tested bacteria was estimated. The tested bacteria that were treated and adjusted to an OD600 of 0.4 were centrifuged (21,000× g for 20 min), using varying doses of sub-MIC. 500 µL of supernatants and fresh erythrocyte suspension (2%) in 0.8 mL saline were combined, and the mixture was incubated for 2 h at 37 °C before centrifuging at 4 °C and 11,000× g for 10 min. A positive control (PC) of complete hemolysis was produced by adding 0.1% of sodium dodecyl sulphate to the suspension of erythrocyte, and a negative control (NC) of unhemolyzed erythrocytes was produced by incubating the erythrocytes in Luria-Bertani (LB) broth at the same conditions. The absorbance at 540 nm was used to estimate the release of hemoglobin. The percentage change in Zn-MnO nanocomposite -induced hemolysis from untreated control cultures was reported for sub-MIC treated tested bacteria[41]. The hemolysis percentage was assessed after comparing the releasing hemoglobin with the positive and negative controls employing the next equation.

$$\text{Hemolysis } (\%) = \frac{\text{ZnO@MnO2 nanocomposite with bacteria} - \text{ NC}}{\text{PC } - \text{ NC}} \times \text{ 100}$$

Docking potential

Molecular docking, a well-recognized and multipurpose in silico technique was used to predict the binding interactions between each protein and the selected ligands. We carried out molecular docking analyses of manganese oxide ($Mn_{12}O_{12}$) and zinc oxide ($Zn_{12}O_{12}$) nanoclusters using a software of Molecular Orbital Environment (MOE) to investigate the binding modes among the ligands and the targeted enzymes (The crystal structure of putative aminohydrolase from MRSA (PDB ID: 4EWT), structure of methicillin acyl-penicillin binding protein 2a from MRSA (PDB ID: 1MWU) and K2U bound crystal structure of class II peptide deformylase from MRSA (PDB ID: 6JFQ). All of the compounds' configurations were drawn with the Gaussian 09 program and saved as MOL files (.mol) for MOE to display[42]. The protein's 3D structure was obtained from the Protein Data Bank (PDB) database (http://www.rcsb.org/pdb, accessed on 15 April 2024) with the respective IDs, respectively 4EWT, 1MWU and 6JFQ. Atoms of hydrogen were included next the water molecules around the protein had been eliminated. The parameters and charges were determined employing the field of MMFF94x force. After creating alpha-site spheres employing MOE's site finder module, we docked our compounds in the active site using MOE's DOCK module. The dock scoring for the MOE program was determined employing the London dG scoring method, with placement as a triangle matcher, retention as 10, and refinement as a force field. The leading conformations of the docked ligands were identified by considering the values of RMSD, binding energies, and modes of binding with the selected residues.

In vitro COX-1 and COX-1 inhibition assay

Following the manufacturer's instructions, the Zn-MnO nanocomposite's in vitro capacity to inhibit COX-1 isoenzymes was assessed using COX 1 and COX 2 inhibitor showing assay kits, which have catalogue numbers of k548 and k547, respectively, from Biovision, USA. In a final volume of 1 ml, the Zn-MnO nanocomposites was dissolved in 1.0% DMSO and tested at doses ranging from 1000 to 0.5 µg/ml, or the vehicle. The COX-1 inhibition assay was conducted using celecoxib as positive controls. GraphPad PRISM was used to calculate the dose of the Zn-MnO nanocomposites causing 50% inhibition (IC_{50}) based on the concentration response curve[43].

Results and discussion

Biosyntheis and characterization of Zn-MnO nanocomposite

In the present investigation, the biocreator of bimetallic Zn-MnO nanocomposite was selected depending on its ability to resist high concentration of precursors of nanocomposite precursors among other isolates.

The utilized extract of *P. rubens* in the synthesis of Zn-MnO nanocomposites was anlaysed via GC-MS, where numerous compounds were identified in the extract (Data not tabulated). GC-MS revealed the presence of Glycine, N-[(3à,5á)-24-oxo-3-[(trimethylsilyl)oxy]cholan-24-yl]-, methyl ester; pentadecylic acid; oleic acid; bromoundecanoic acid; palmitic acid, ethyl ester; oxiraneoctanoic acid, 3-octyl-, cis-; stearin, 2-mono-; tetradecamethylheptasiloxane; hexadecanoic acid, 1-(hydroxymethyl)-1,2-ethanediyl ester; propanoic acid, 2-(3-acetoxy-4,4,14-trimethylandrost-8-en-17-yl)-; and Glycerol 1-palmitate, 9(11)-Dehydroergosterol tosylate;

and heptasiloxane. Theses metabolites may functionlized as stabilizing and reducing agents for Zn-MnO nanocomposite synthesis as mentioned recently[7,44].

Several techniques were applied to characterize and document the formation of NPs, from which UV–Vis spectroscopy, that is widely utilized to detect the optical properties of created NPs via recognizing a suitable absorption peak[11]. From the Fig. 1a, the maximum absorbance beak of formulated Zn-MnO nanocomposites was recorded at 370 nm by UV–Vis spectroscopy. The obtained spectrum of UV–Vis indicates that the process of MnO-ZnO nanocomposite creation of was achieved. According to the earlier study of Martínez-Vargas et al.[45], the synthesized Zn-MnO nanocomposite was detected at absorption spectrum 371 nm. Recently, EL-Moslamy et al.[16] revealed the UV–Vis spectra of formulated MnO-ZnO nanocomposite was at 350 to 400 nm.

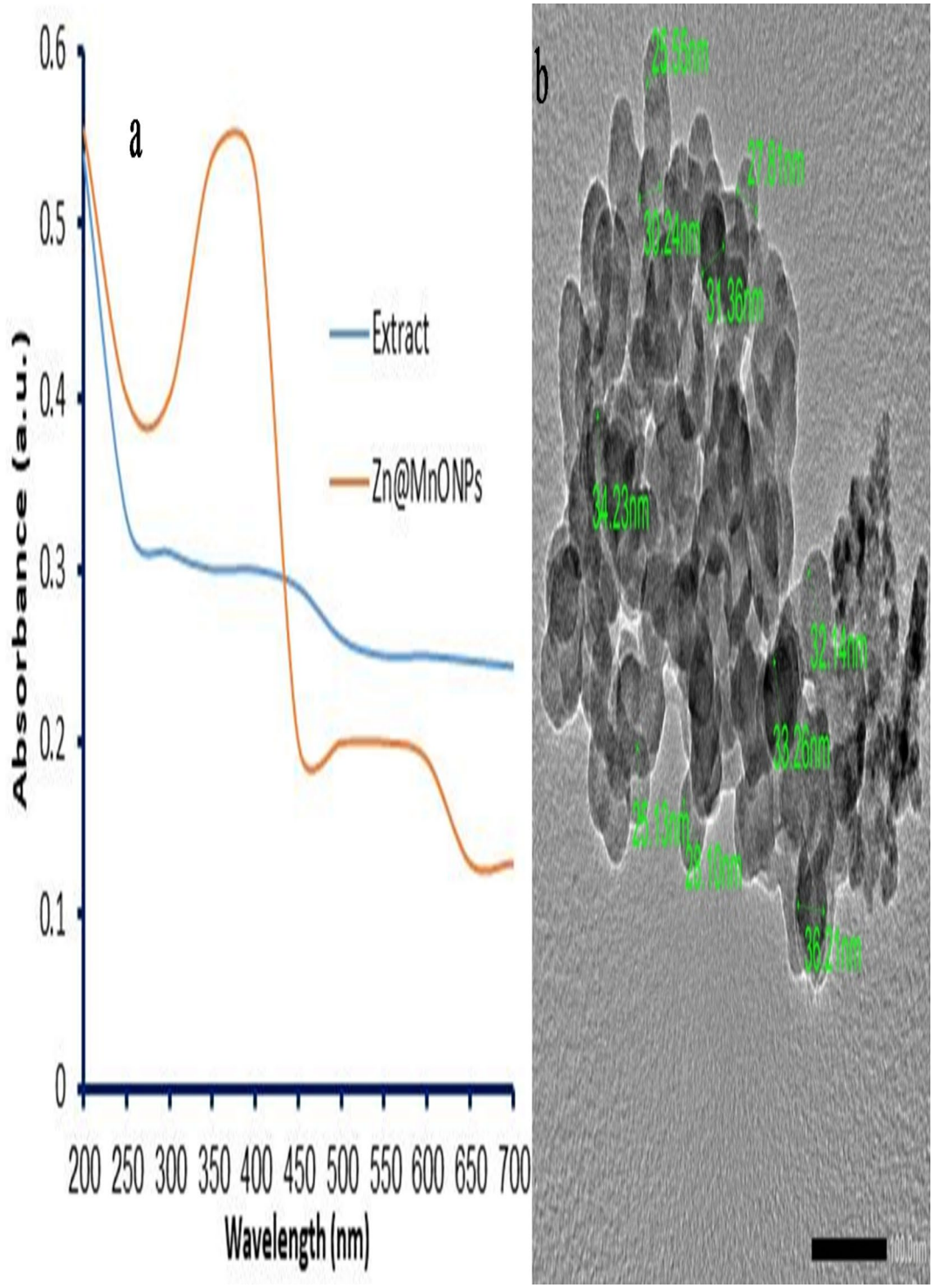

Fig. 1. UV–Vis spectroscopy (**a**) and TEM (**b**) characterization of biosynthesized Zn@MnO nanocomposites.

The size and shape of formulated Zn-MnO nanocomposite were characterized by TEM with irregular and spherical-like shape and diameter average of 25.13 to 36.21 nm (Fig. 1b). According to the result of Anantha et al.[24], ZnO-MnO_2 nanocomposite was visualized in a mixture of spherical (MnO_2) and cubical (ZnO) dots with clustered agglomerates. The shape and size are dependent on synthesis method, reducing and capping agents that employed in synthesis of MnO-ZnO nanocomposite[46]. In the current investigation, TEM appeared agglomeration of MnO-ZnO nanocomposite. According to Alagesan et al.[47], the agglomerated nanoparticles possess higher biological activities.

The use of FTIR was employed to authorize that functional groups existed on the surface of biosynthetic CuO-ZnO nanocomposite materials Fig. 2. The characteristic peak of the amide I band (C=O stretch/hydrogen bond joined with COO–) is appointed to a frequency of 1674 cm^{-1}, as the spectra show. On the other hand, the amide II band (NH bending joined with CN stretching) is apportioned to frequencies of 1430, 1367, and 1226 cm^{-1} (COO– symmetrical stretching). The C-O stretching frequency at 1036 cm^{-1} is linked to the amide III band. They attribute the peaks at 3417 and 2949 cm^{-1} to OH and -COO stretching, respectively. The metal–oxygen vibration (Mn–O and Zn-O) is represented by the peak positions at 862, 614, 538, and 431 cm^{-1} frequencies[48,49].

The XRD patterns are employed to analyze the crystalline nature as well as phase purity of the created Zn-MnO nanocomposites. Figure 3 shows the X-ray diffraction spectra of sample (Zn-MnO nanocomposites). The sample contained two distinct components, MnO (JCPDS 81-2261) and ZnO (JCPDS 36-1451), without any additional impurity peaks[50]. MnO-ZnO nanocomposite showed peaks emerged at 2θ = 27.6°, 56.64°, and 72.83° corresponding to (110), (211), and (301) planes of the MnO crystal structure, correspondingly. On the other hand, plane of ZnO crystal structure peaks emerged at 2θ = 31.8, 34.44, 36.33, 47.59, 62.9 and 69.19°, which corresponded to (100), (002), (101), (102), (103), and (112)[9,49,51,52]. The diffractogram of the Zn-MnO

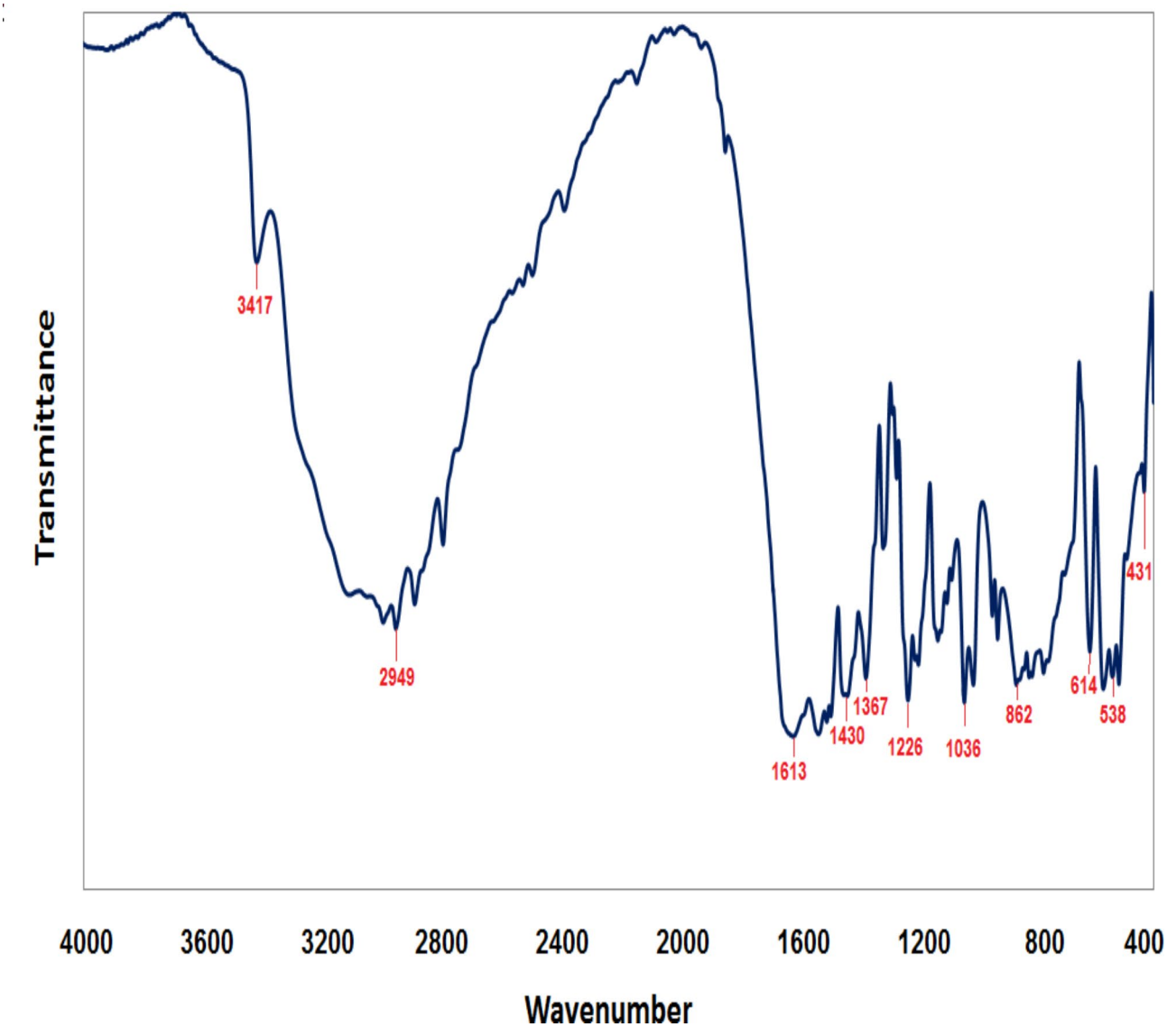

Fig. 2. FT-IR spectra of Zn-MnO nanocomposite.

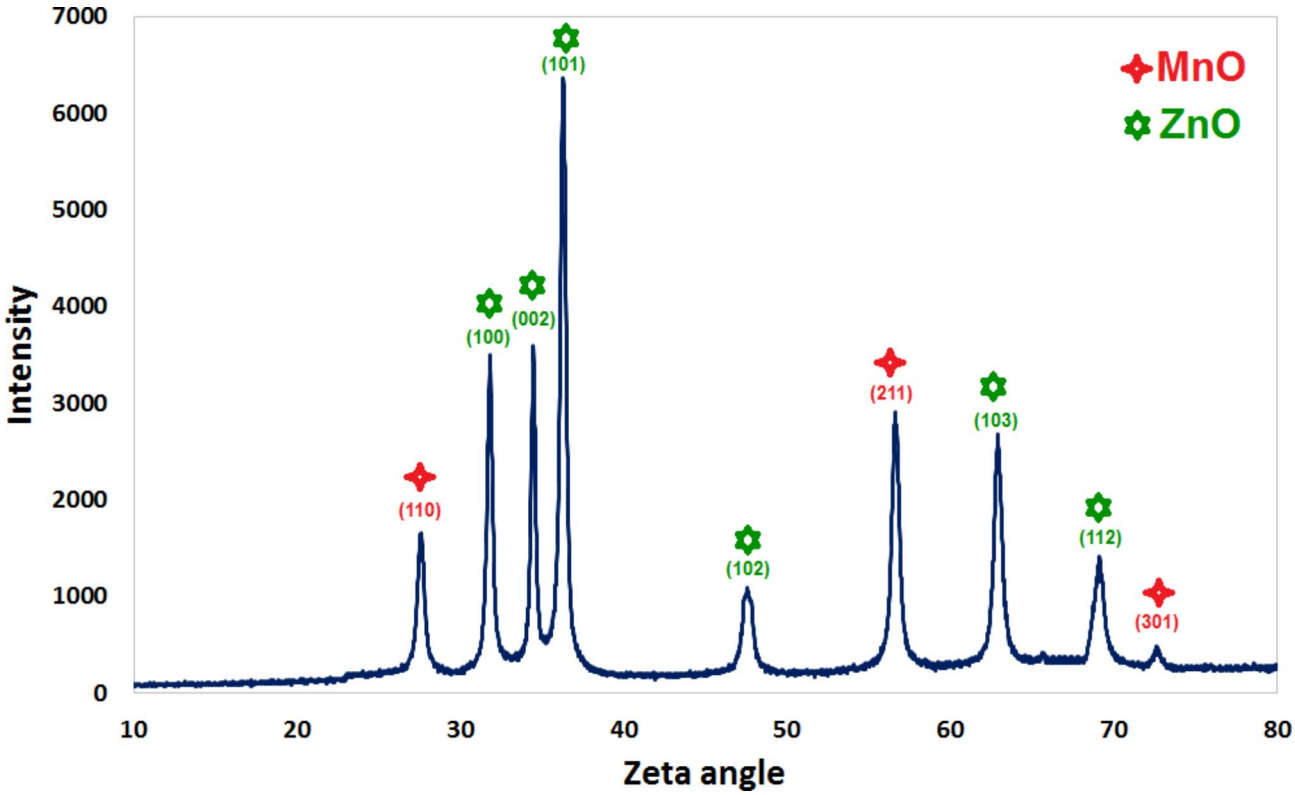

Fig. 3. XRD pattern of Zn-MnO nanocomposite.

nanocomposites does not indicate the presence of any further contaminants. It guarantees the purity of the resulting Zn-MnO nanocomposite.

As visualize in Fig. 4, the SEM was employed to assess the surface morphology of Zn-MnO nanocomposite. Zn-MnO nanocomposites had a shape that was virtually irregular. EDX analysis was employed to assess the elemental structure of the CuO-ZnO nanocomposite. In the Zn-MnO nanocomposite, the EDX spectra showed the presence of numerous well-defined elements related to manganese [Mn], Zinc [Zn], oxygen [O], besides carbon [C] components (Fig. 4). The carbon [C] in sample from the metabolites, whereas the manganese [Mn], Zinc [Zn], oxygen [O] indicate the formation of Zn-MnO nanocomposite.

The stability of Zn-MnO nanocomposite in aqueous suspension was documented via zeta potential investigation which provided value − 15.6 mV (Fig. 5a). Recent investigation found that the value of zeta potential was − 25.2 mV which confirmed the stability property of mycosynthesized ZnO-MnO nanocomposite[16]. The dimension of ZnO-MnO nanocomposite was also detected via DLS which revealed its size ranged from 50 to 70 nm (Fig. 5b). The detected size of ZnO-MnO nanocomposite via DLS match well with the TEM investigation which indicated that composite is found in nanoscale form.

Antimicrobial activities of Zn-MnO nanocomposite

The recorded inhibition zones indicated that Zn-MnO nanocomposite was more effective than positive control against all examined bacteria but with different levels based on the bacterial species (Table 1; Fig. 6). *S. aureus* was the most sensitive to Zn-MnO nanocomposite followed by *S. typhi*, MRSA, and *K. pneumoniae* with inhibition zones 36 ± 0.1, 27 ± 0.2, 25 ± 0.1, 23 ± 0.2 mm, respectively. In support of this investigation, Zn-MnO nanocomposite at 300 µg/mL were found to have cidal activity towards several bacteria namely *Shigella flexneri*, *Escherichia coli*, *Bacillus megaterium*, *Salmonella typhimurium*, and *Bacillus subtilis*[48]. Antibacterial, antifungal, and antioxidant of Zn ONPs were reported[53]. According to EL-Moslamy et al.[16], *Salmonella paratyphi* was the most sensitive to Zn-MnO nanocomposites with inhibition area of 53.17 mm at 90 µg/mL. Also, *Pseudomonas aeruginosa* was sensitive to Zn-MnO nanocomposites with large inhibition zone (49.3 mm) at 10 µg/mL. Additionally, the recorded inhibition zones were 24.28 and 39.2 mm at 130 µg/mL of Zn-MnO nanocomposites toward *S. aureus* and *Bacillus cereus*. Moreover, low MIC (15.62, 31.25, and 31.25 µg/mL) and MBC (31.25, 62.5, and 125 µg/mL) quantities of Zn-MnO nanocomposite were detected against tested bacteria (*S. aureus*, MRSA, and *S. typhi*), respectively while *K. pneumoniae* was the most tolerance with 125 µg/mL of MIC and MBC. Al Abboud et al.[54] reported high quantity of ZnO-AuNPs MIC ranged from 62.5, to 125 µg/mL versus *E. coli*, *S.aureus*, and *S. typhi*), respectively. The ratio of MBC/MIC was ≤ 4 at all tested bacteria indicated its bactericidal effect. According to EL-Moslamy et al.[16], 10, 90, and 130 µg/mL were the MICs of Zn-MnO nanocomposites against *P. aeruginosa*, *S. paratyphi*, and *B. cereus*, respectively. While 100, 150, and 200 µg/mL were the MBCs of Zn-MnO nanocomposites against *P. aeruginosa*, *S. aureus* and *S. paratyphi*, respectively.

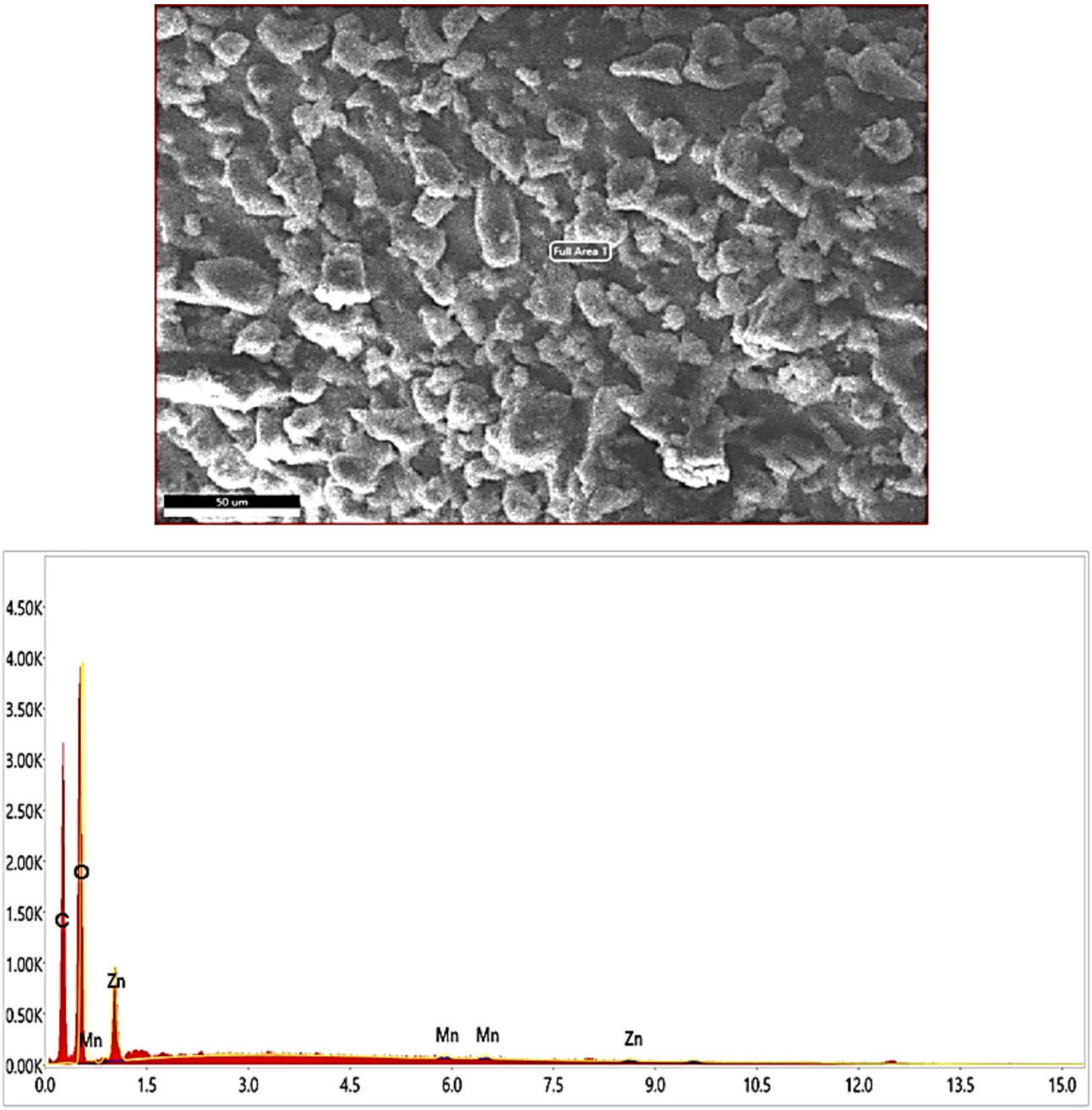

Fig. 4. SEM-EDX analysis of Zn-MnO nanocomposite.

Typek et al.[28] and Ogunyemi et al.[55] mentioned that the utilization of individual MnO NPs and ZnO NPs to inhibit the pathogenic bacteria reflected less inhibition than its nanocomposite because if it's large crystalline size. Our Zn-MnO nanocomposite exhibited better antimicrobial activities besides it ecofriendly and safe if compared to other individual metals oxide NPs. To our knowledge, Ag NPs is toxic compared to Zn or MnO NPs. In case the antimicrobial activity, the obtained inhibition zones in the current study were higher than recorded using other metal NPs, for instance the mycosynthesized Ag NPs inhibited *S. typhi* and *S. aureus* with inhibition zones of 14.41 ± 1.7 mm and 18.21 ± 2.1 mm, respectively[56], the mycosynthesized CdO NPs inhibited *B. cereus*, *P. aeruginosa*, and *E. coli* with inhibition zones of 7.5 ± 0.2, 19.6 ± 0.6, and 17.6 ± 0.4 mm, respectively[57]. Moreover, Alghonaim et al.[39] reported the antimicrobial potential of CuO-Au nanocomposite against *C. albicans*, *E. coli*, and *E. faecalis* with 8, 15, and 27 mm, respectively of inhibition area. Antibacterial, antifungal, and antioxidant of Zn ONPs were reported[53]. Recently the mycosynthesized ZnO-MnO nanocomposite (210 µg/mL) via *Clonostachys rosea* inhibited different microorganisms including yeasts (*Candida albicans* and *C. tropical* with 7.32 and 10.65 mm of inhibition zones, respectively) and bacteria (*Staphylococcus epidermidis*, *E. coli*, *S. aureus*, *Streptococcus pneumoniae*, *P. aeruginosa*, and *K. pneumoniae* with 25.63, 11.21, 15.68, 18.45, 14.04, and

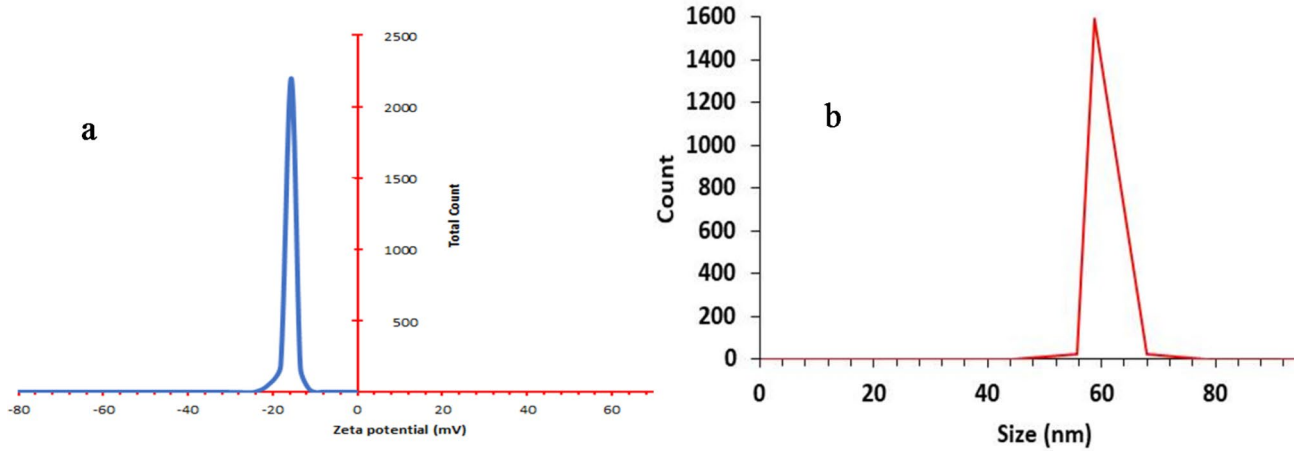

Fig. 5. Characterization of ZnO-MnO nanocomposite via zeta potential analysis (**a**) and DLS for size detection (**b**).

Tested bacteria	Inhibition zone (mm)			Zn-MnO nanocomposite (µg/mL)		MBC/MIC (µg/mL)
	Zn-MnO nanocomposite	+ve Control	-ve Control	MIC	MBC	
S.aureus	36 ± 0.1	32 ± 0.3	0.0	15.62	31.25	2
MRSA	25 ± 0.1	23 ± 0.2	0.0	31.25	62.5	2
K. pneumoniae	23 ± 0.2	19 ± 0.1	0.0	125	125	1
S. typhi	27 ± 0.2	25 ± 0.3	0.0	31.25	125	4

Table 1. Antimicrobial activity of Zn-MnO nanocomposite. +ve, positive; −ve, negative.

19.36 mm of inhibition zones, respectively)[16]. The obtained results in the present work were compared with other studies as illustrated in Table 2.

K. pneumoniae was selected as a model of tested bacteria to evaluate the action mechanism of Zn-MnO nanocomposite. The untreated *K. pneumoniae* by Zn-MnO nanocomposite showed identical rod form with clear cell wall, cell membrane, and cytoplasmic contents, while treated cells showed irregular form with thin wall, several vacuoles, and collapse of cell membrane far from cell wall, besides the rupture of cell wall (Fig. 7). The high antibacterial activity of Zn-MnO nanocomposites perhaps due to the nature of Zn dispersion matrix of MnO_2 .Furthermore, the integration advantage of Zn into lattice of MnO_2 may slowly the releasing free ions and therefore increases their activity as mentioned in the incorporation of Silver-doped Mg NPs[58]. The mechanism of bacterial inhibition by NPs involves the attachment between cell wall and NPs, membrane damage, and distortion in respiration pathways as mentioned in numerous studies. The differences among the level of bacteria may depend on several factors such as cell wall composition, dose, type, and synthesis source of NPs. Saqib et al.[56] mentioned that NPs enjoy with big surface area which assist it's the antimicrobial ability.

The biofilm formation of tested bacteria was examined at different sub-doses (MIC) of Zn-MnO nanocomposite (Fig. 8). The inhibition level of biofilm increased with the increasing the tested dose, where the antibiofilm was 82.07, 75.43,43.65, and 41.35% at 25% MIC while it was 96.54, 93.0, 94.53, and 91.11% at 75% MIC against *S. aureus*, MRSA, *K. pneumoniae*, and *S. typhi*, respectively. At 75% MBC, the biofilm of *S. aureus* was the most affected followed by *K. pneumoniae*, MRSA, and *S. typhi*. Surprisingly, antibiofilm % at 25% MBC was very low for *K. pneumoniae* and *S. typhi* if compared to *S. aureus* and MRSA. According to Abdelraheem et al.[29], there was a positive correlation among the levels of biofilm development inhibition and dose of ZnO NPs. Recently, ZnO doped with Mn demonstrates antibacterial activity towards *S. aureus* and *E. coli*. The inhibition zones were varies amongst bacterial species. Furthermore, compared to *E. coli*, the growth of *S. aureus* displayed greater fluctuation at all concentrations. Moreover, the inhibition rises with the Mn-doped ZnO composite concentration[63]. Inhibition of exopolysaccharide synthesis represents one of the action mechanisms of ZnO NPs against bacterial biofilm formation[41], also, biofilm matrix are destroyed by ZnO NPs due to their small size.

From the clinical investigations by several authors, some serious problems coming from the bacterial toxins. These toxins joined to the membranes of erythrocytes and cause blood hemolysis such as such as *S. aureus* α-Toxin[64]. So, the influences of Zn-MnO nanocomposite s on blood hemolysis by *S. typhi*, MRSA, *K. pneumoniae*, and *S. typhi* were investigated currently. It's demonstrated that MIC % (25–75% of Zn-MnO nanocomposite) prevent the hemolysis but with various degrees depending on the tested bacteria species as well as the applied dose (Figs. 9 and 10). Low effect of Zn-MnO nanocomposite s at 25%, 50%, and 75% MIC was recorded on the hemolysis inhibition of 37.9, 56.4, and 89.1%, respectively with the presence of *K. pneumoniae*, but the high effect was observed with the presence of MRSA with hemolysis inhibition of 53.2, 91.8, and 96.3%, respectively.

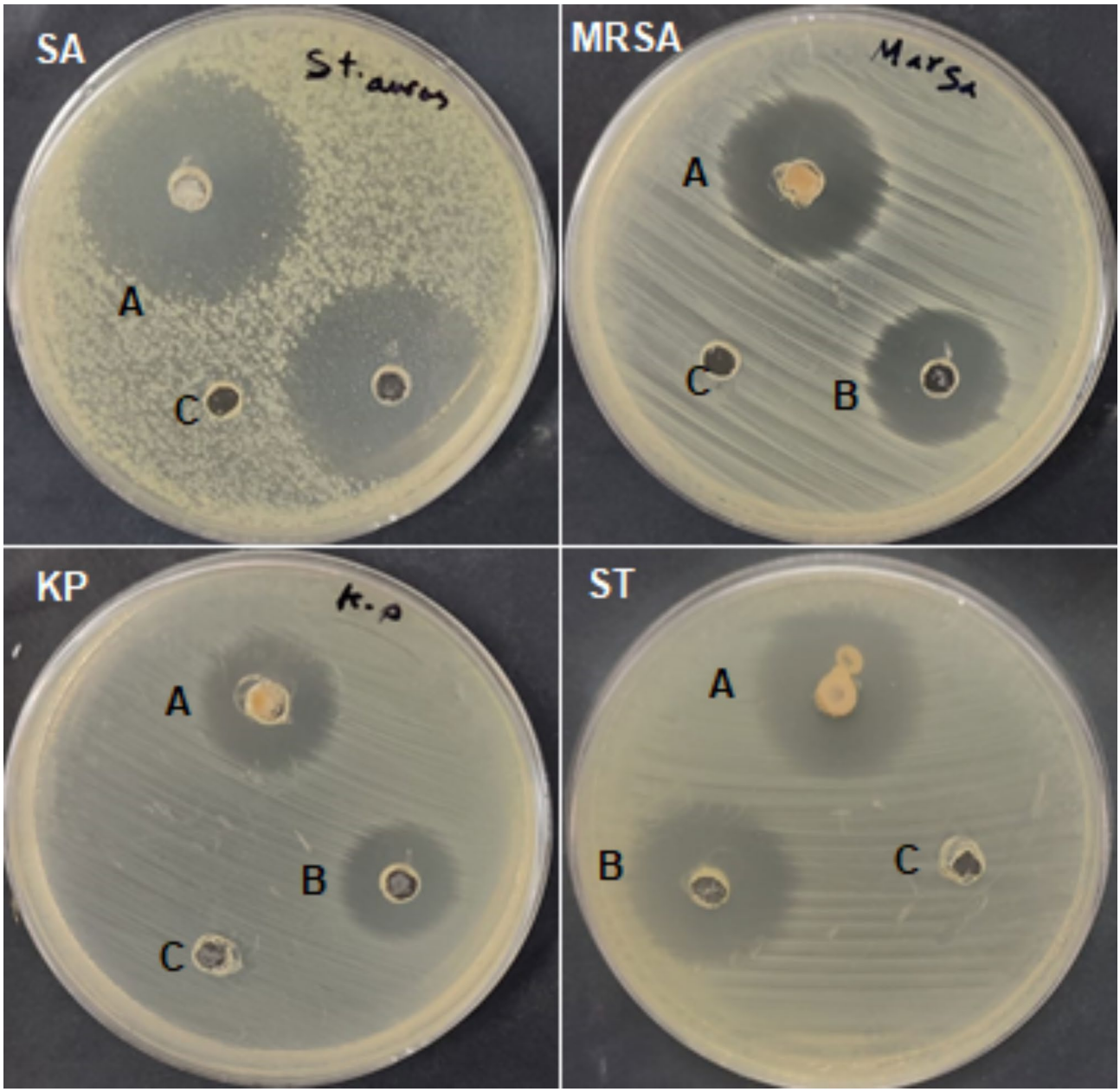

Fig. 6. Inhibition zones of tested bacteria treated by Zn-MnO nanocomposite (A), positive control (B) and negative control (C). *S. aureus* (SA), MRSA, *K. pneumoniae* (KP), and *S. typhi* (ST).

Hemolysis inhibition in our findings by Zn-MnO nanocomposite in the existence of tested bacteria has main suggestions in relation to the bacteria virulence's control. The other results were documented about inhibition (%) of hemolysis in the occurrence of *S. aureus* and *S. typhi* (Fig. 9). Findings of Salem et al.[65] signified the anti-hemolytic potential of ZnO NPs. In another report[66], hemolytic potential of *P. aeruginosa* was influenced by ZnO NPs through decrease of virulence factors production like protease, pyocyanin, and hemolysin.

Molecular modeling: docking investigation

The molecular docking investigations were employed to manganese oxide ($Mn_{12}O_{12}$) and zinc oxide ($Zn_{12}O_{12}$) NPs (MnO NPs and ZnO NPs) against MRSA. The three-dimensional crystal structure of putative aminohydrolase (PDB ID: 4EWT), structure of methicillin acyl-penicillin binding protein 2a (PDB ID: 1MWU), and K2U bound crystal structure of class II peptide deformylase (PDB ID: 6JFQ) were used as the biological targets for the docking analysis. The data were gathered in Tables 3 and 4, revealing a high agreement between docking and experimental results.

Docking of MnO NPs and ZnO NPs into modeled receptors was undertaken to determine an optimal orientation of nanoparticles, including non-covalent interactions between the receptor's active site and NPs. This led to the production of novel medications for future biological study.

NPs	Particle size (nm)	Concentration (µg/mL)	Tested strain	Inhibition zones (mm)	MIC µg/mL	Method of synthesis	References
Zn-MnO nanocomposites	19.69 to 26.41	300	*E. coli*	28	ND	Co-precipitation	48
MnO NPs	10 to 23	50	*B. cereus* and *E. coli*	18 to 20	15 to 25	Biological via *B. subtilis*	59
MnO NPs	20.84	50	*E. coli* and *S.aureus*	15 to 21	ND	Biological via *Tagetes erecta*	60
Ruthenium-doped MnO NPs	50	100	*E. coli*, *K. pneumonia*, and *S. aureus*	13 to 26	ND	Microwave-assisted hydrothermal	61
MnO NPs	23.62	100	*E. coli* and *S. aureus*	3 to 12	ND	Biological Coriandrum sativum extract	62
ZnO-Au NPs	15	100	*S.aureus*, *E. coli*, and *S. typhi*	15 to22	62.5, to 125	Biological via *P. crustosum*	54
ZnO NPs	5–43 nm	100	*S. aureus* and *K.pneumoniae*	23.83 and 23.83	ND	Biological via *Salix tetrasperma*	9
CuO-Au NPs	20	100	*E. coli* and *E. faecalis*	16 to 27	31.25 to 62.5	Biological via *P. crustosum*	39

Table 2. Antibacterial properties of different NPs based on published papers.

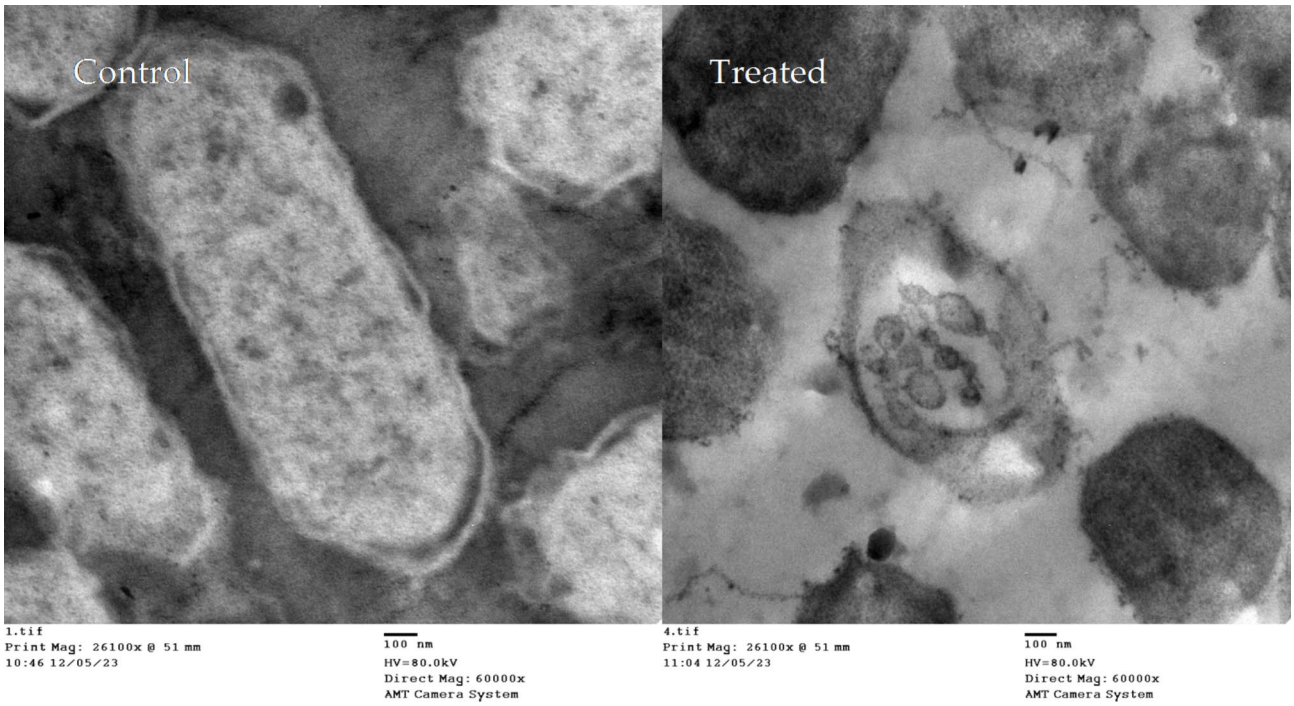

Fig. 7. Effect of Zn-MnO nanocomposite on ultrastructure of *K. pneumoniae*.

MnO-NPs and ZnO-NPs demonstrated efficient in silico suppression of all examined proteins with low docking scores and acceptable RMSD values.

(1) Docking MnO NPs and ZnO NPs with (4EWT) active sites indicated a higher negative score of free binding energy (-3.26648 kcal/mol) of ZnO NPs and binding interactions with the residues (SER 332 and GLU 139).

(2) MnO-NPs and ZnO-NPs were ranked as good effective inhibitors to (1MWU) protein with docking scores − 2.53804 and − 2.25577Kcal/mol respectively.

(3) 6JFQ protein was observed that MnO NPs showed a stronger binding energy of (-2.97631 kcal/mol) than that of ZnO-NPs (-1.67551 kcal/mol). MnO NPs bounded with (6JFQ) through amino acid residues GLU 21 via Mn 5, O 1, and O 2 atoms.

Molecular docking of other bimetallic of Ag–Cu nanocomposite against β-lactamase enzyme responsible for cell wall biosynthetic pathway in *S. aureus* resulted Binding score of − 4.981 kcal/mol[67]. Additionally, El-Sayed et al.[68] applied the molecular docking interaction among the Penicillin-binding proteins (PBPs) (a key a group of enzymes which play a critical role in cell wall synthesis in *S. aureus*) and Cu-doped ZnO. Who study reflected Binding score of − 7.90 kcal/mol for penicillin-binding protein. Also, Al-Rajhi et al.[69] confirmed the activity of NPs (CuO NPs and FeO NPs) against different yeasts via MD interaction. Figure 11a–f depicts the best-fitted 2D and 3D postures selected by the studied NPs, while Table 3 presents the binding energy values. A list of hydrogen bonds between MnO NPs and ZnO NPs with examined proteins is respectively presented in Table 4. The binding

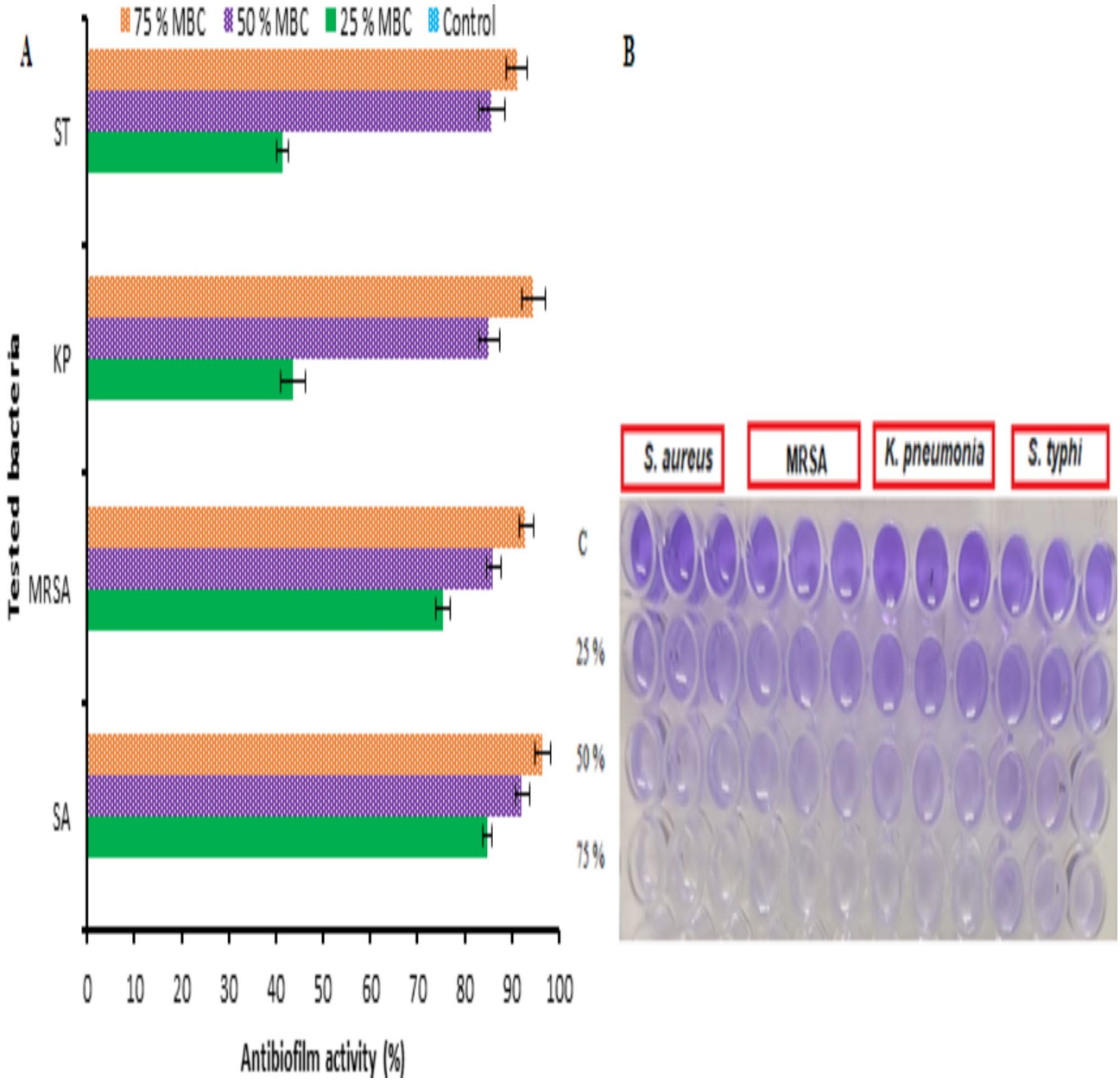

Fig. 8. (**A**) Antibiofilm activity of Zn-MnO nanocomposite against *S. aureus* (SA), MRSA, *K. pneumoniae* (KP), and *S. typhi* (ST). (**B**) Microtiter plate offered color shifts as a pointer of decreased test bacteria viability. Media amended by bacteria (C), media amended by bacteria and 25% of MBC of Zn-MnO nanocomposite, media amended by bacteria and 50% of MBC of Zn-MnO nanocomposite, media amended by bacteria and 75% of MBC of Zn-MnO nanocomposite.

proteins connect with examined NPs by stabilizing them in the receptor's cavity of amino acid, preventing the development of the targeted proteins. Figure 12 demonstrated the forms key of interaction among ZnO NPs/MnO NPs and receptors of protein.

Anti-inflammatory activity of Zn-MnO nanocomposite

Since there are ethical concerns about using animals for research when there are other suitable methods available for analysis, it can be very difficult to conduct experiments on animals at times. In order to assess the anti-inflammatory potential of Zn-MnO nanocomposite, an inhibition assay of cyclooxygenase-1 (COX-1) and cyclooxygenase-2 (COX-2) enzymes was carried out. Arachidonic acid is converted by the enzymes to prostaglandin (PG) H2, which is the construction block of PGs and thromboxane. These lipid mediators are essential for processes of normal physiology and inflammation as well as pain[32]. The inhibitory potential of Zn-MnO nanocomposite on COX-1 and COX-2 Enzymes was remarked but with various levels depending on the kind of enzyme. The level of inhibition increased with increasing the dose of Zn-MnO nanocomposite up

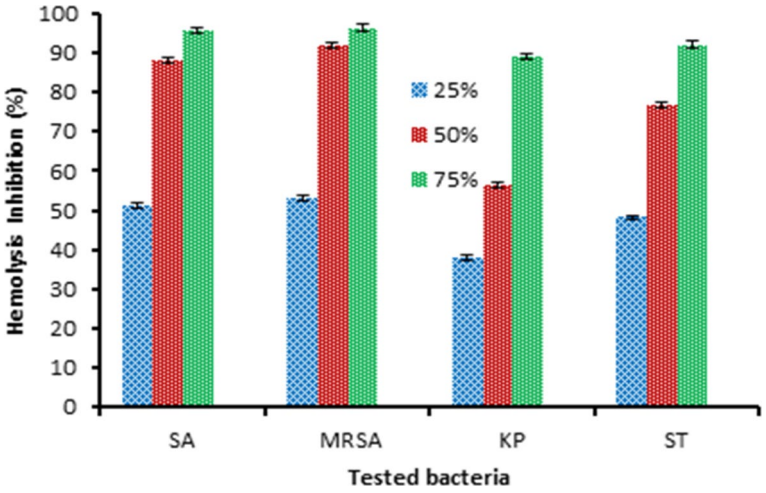

Fig. 9. Hemolysis inhibition of Zn-MnO nanocomposite (At different doses 25%, 50%, and 75% of MIC) in the occurrence of *S. aureus* (SA), MRSA, *K. pneumoniae* (KP), and *S. typhi* (ST).

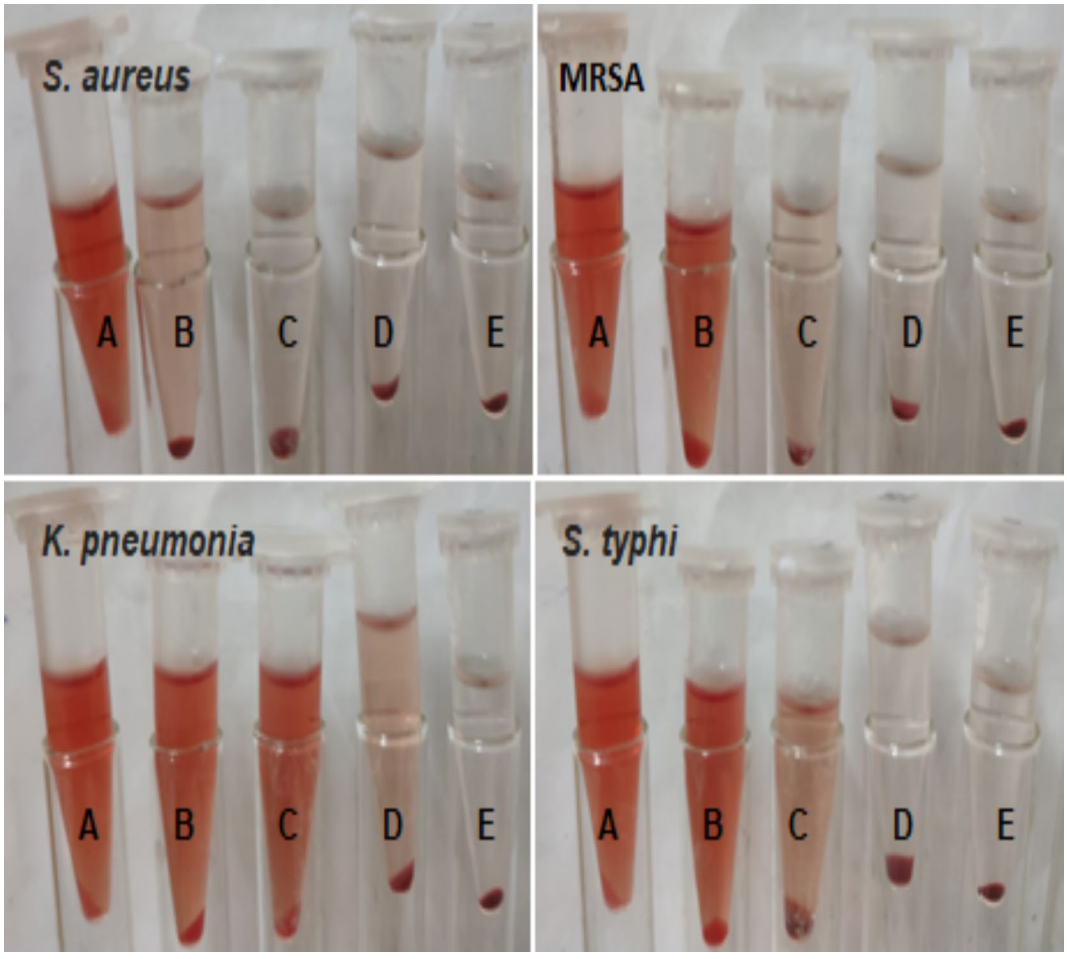

Fig. 10. Blood hemolysis treated by Zn-MnO nanocomposite in the existence of *S. aureus*, MRSA, *K. pneumoniae*, and *S. typhi*. (A, Negative control; B, 25% MIC dose; C, 50% MIC dose; D, 75% MIC dose; and E, positive control)

Mol	Protein	S	rmsd_refine	E_conf	E_place	E_score1	E_refine	E_score2
MnO NPs	4EWT	− 2.18846	1.142505	− 1807.66	− 37.4001	− 4.53014	159.2952	− 2.18846
ZnO NPs	4EWT	− 3.26648	2.258528	− 1118.69	− 40.8527	− 3.63705	8.859861	− 3.26648
MnO NPs	1MWU	− 2.53804	2.970423	− 2053.05	− 47.038	− 4.92198	21.95385	− 2.53804
ZnO NPs	1MWU	− 2.25577	3.251037	− 1113.63	− 37.0092	− 5.50074	− 32.455	− 2.25577
MnO NPs	6JFQ	− 2.97631	1.580399	− 2057.53	− 22.0367	− 7.60384	6.997857	− 2.97631
ZnO NPs	6JFQ	− 1.67551	1.235317	− 1164.1	− 4.36152	− 9.54607	− 1.57651	− 1.67551

Table 3. Docking scores and energies of MnO NPs and ZnO NPs with methicillin-resistant *S. aureus* (PDB ID: 4EWT, 1MWU and 6JFQ) receptors.

Mol	Protein	Ligand	Receptor	Interaction	Distance	E (kcal/mol)
MnO NPs	4EWT	Mn 5	SG CYS 103 (A)	H-donor	2.94	− 0.7
		Mn 3	O SER 332 (A)	Metal	2.36	− 1.9
		Mn 15	OE1 GLU 139 (A)	Metal	2.42	− 3.2
		O 7	OE1 GLU 138 (A)	Ionic	2.72	− 6.6
ZnO NPs		O 14	N SER 332 (A)	H-acceptor	2.93	− 0.6
	4EWT	Zn 9	O SER 332 (A)	Metal	2.42	− 1.8
		O 5	OE1 GLU 139 (A)	Ionic	3.77	− 1.0
MnO NPs	1MWU	–	–	–	–	–
ZnO NPs	1MWU	O 14	NZ LYS 430 (A)	H-acceptor	3.18	− 0.5
		Zn 2	OE1 GLU 602 (A)	Metal	2.00	− 2.6
		O 1	OE1 GLU 602 (A)	Ionic	3.01	− 4.4
		O 1	OE1 GLU 602 (A)	Ionic	3.99	− 0.5
MnO NPs	6JFQ	Mn 5	OE2 GLU 21 (A)	Metal	2.61	− 1.1
		O 1	OE2 GLU 21 (A)	Ionic	3.96	− 0.6
		O 2	OE2 GLU 21 (A)	Ionic	3.14	− 3.6
ZnO NPs	6JFQ	Zn 10	OE2 GLU 21 (A)	H-donor	2.90	− 0.5
		Zn 4	OE2 GLU 21 (A)	Metal	2.05	− 3.9
		O 1	OE2 GLU 21 (A)	Ionic	3.84	− 0.9
		O 3	OE1 GLU 21 (A)	Ionic	3.26	− 2.9

Table 4. MnO-NPs and ZnO-NPs interaction with methicillin-resistant *S. aureus* (PDB ID: 4EWT, 1MWU and 6JFQ) receptors.

to 1000 µg/mL. COX-1 enzyme was more affected with IC_{50} 20.81 ± 0.68 µg/mL than COX-2 Enzyme with IC_{50} 35.87 ± 1.35 µg/mL. However, IC_{50} value of Celecoxib was less (3.65 ± 0.19 µg/mL) on COX-2 enzyme compared to its values (6.05 ± 0.61 µg/mL) on COX-1 enzyme (Table 5).

Conclusion and future applications

The current investigation focuses the biosynthesis of Zn-MnO nanocomposite from *T. asperellum*. UV–visible spectroscopy, TEM, FTIR, XRD, and SEM with EDX were used to characterize the created Zn-MnO nanocomposite. Our findings emphasize that Zn-MnO nanocomposite can be employed as efficient against multidrug resistance bacteria. This vital function was confirmed via well diffusion method, antibiofilm, hemolysis inhibition in the presence of pathogenic bacteria, and docking interaction. Based on our outcomes, we can mentioned that utilize of Zn-MnO nanocomposite is effective against inflammation via inhibition of COX-1 and COX-2. MnO-NPs and ZnO-NPs with the finest docking scores revealed some flexibility that might influence function and catalytic activities, indicating that they can help with the design and development of new therapies. Future research on the effect of Zn-MnO nanocomposite reactive oxygen species (ROS) which are responsible for microorganisms death in microbial will be suggested, and other mechanisms on molecular levels were recommended. To date, the reported antimicrobial and anti-inflammatory investigations of Zn-MnO nanocomposite were performed in vitro. Greatly attempt is desired for perform in vivo investigations to validate the way for future pharmacological applications of Zn-MnO nanocomposite. Morover, for future theraputic utilizations of Zn-MnO nanocomposite, numerous guidelines are of great significant such as labeling ZnO nanomaterials with radionuclides with studying its pharmacokinetics. It is predictable that study in pharmcological utilization of Zn-MnO nanocomposite will continue to increase over the current decade for several application.

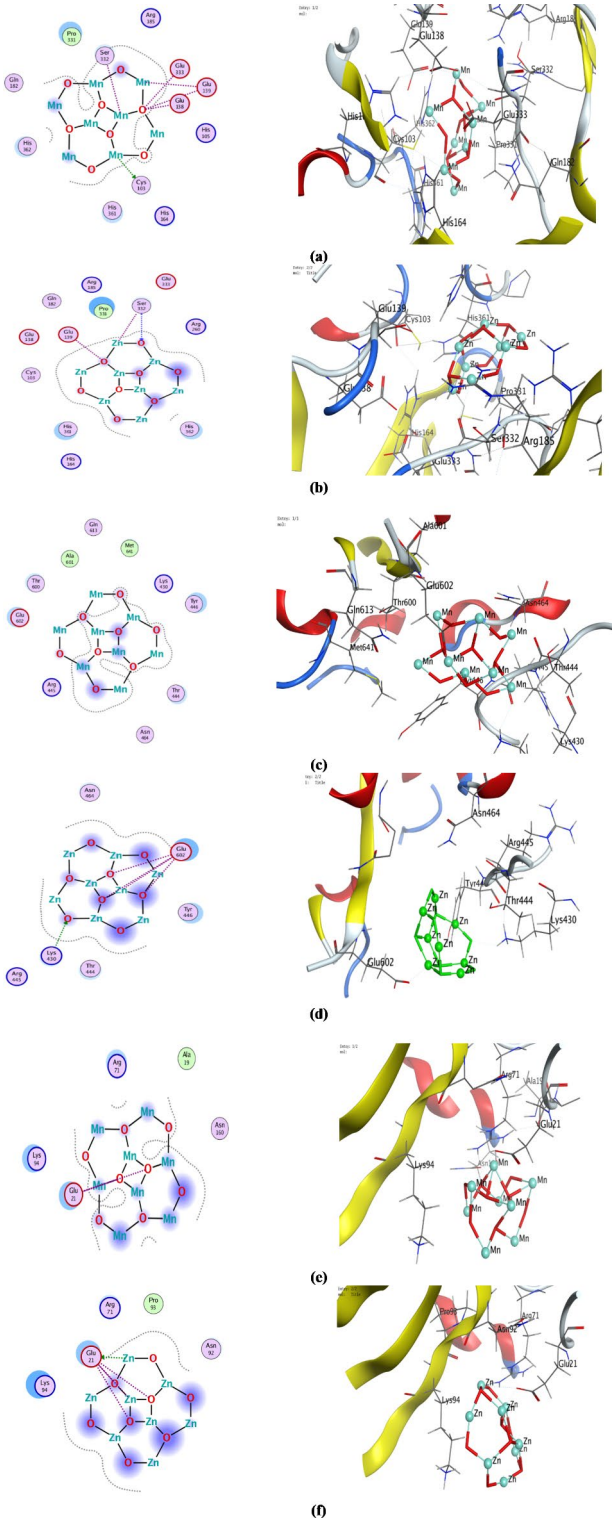

Fig. 11. (**a**) 2D and 3D plans indicate the interaction between MnO NPs and active sites of 4EWT protein. (**b**) 2D and 3D plans indicate the interaction between ZnO NPs and active sites of 4EWT protein. (**c**) 2D and 3D plans indicate the interaction between MnO NPs and active sites of 1MWU protein. (**d**) 2D and 3D plans indicate the interaction between ZnO-NPs and active sites of 1MWU protein. (**e**) 2D and 3D plans indicate the interaction between MnO NPs and active sites of 6JFQ protein. (**f**) 2D and 3D plans indicate the interaction between ZnO NPs and active sites of 6JFQ protein.

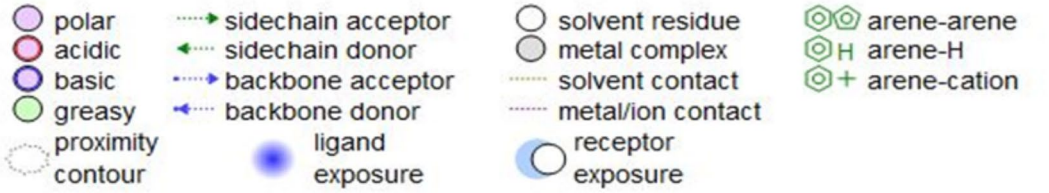

Fig. 12. The demonstrative key for the forms of interaction among ZnO NPs/ MnO NPs and receptors of protein.

	COX-1 Enzyme				COX-2 Enzyme			
	Zn-MnO nanocomposite		Celecoxib		Zn-MnO nanocomposite		Celecoxib	
Conc. (µg/mL)	Activity (%)	Inhibition (%)	Activity (%)	Inhibition (%)	Activity (%)	Inhibition (%)	Activity (%)	Inhibition (%)
1000	5.64	94.36±0.92	3.83	96.17±0.45	12.77	87.23±1.09	2.05	97.95±0.71
500	10.83	89.17±1.35	6.72	93.28±0.54	18.06	81.94±0.89	4.52	95.48±0.64
250	14.88	85.12±1.24	9.29	90.71±0.43	25.42	74.58±0.61	8.12	91.88±0.59
125	21.66	78.34±0.88	13.88	86.12±0.68	31.68	68.32±0.46	12.22	87.78±0.75
62.5	29.58	70.42±1.37	19.57	80.43±0.79	40.73	59.27±1.35	19.57	80.43±1.08
31.25	42.19	57.81±1.79	26.84	73.16±0.92	51.61	48.39±0.75	25.92	74.08±0.26
15.6	53.92	46.08±1.36	31.97	68.03±1.51	58.73	41.27±1.32	32.58	67.42±1.08
7.8	62.87	37.13±0.95	43.76	56.24±1.48	66.15	33.85±0.91	39.65	60.35±0.81
3.9	69.59	30.41±0.73	57.69	42.31±0.95	75.02	24.98±0.68	47.92	52.08±1.44
2	78.06	21.94±0.82	61.98	38.02±0.74	83.28	16.72±0.34	59.77	40.23±0.96
1	85.25	14.75±0.73	69.55	30.45±0.81	90.14	9.86±018	66.83	33.17±0.61
0.5	89.77	10.23±0.41	76.41	23.59±0.53	93.79	6.21±0.35	72.11	27.89±0.57
0	100	0.0±0.0	100	0.0±0.0	100	0.0±0.0	100	0.0±0.0
IC_{50}	20.81 ± 0.68 µg/mL		6.05 ± 0.61 µg/mL		35.87 ± 1.35 µg/ml		3.65 ± 0.19 µg/mL	

Table 5. Anti-inflammatory potential of Zn-MnO nanocomposite.

Data availability

The results from the present investigation are available from the corresponding author upon reasonable appeal.

Received: 29 August 2024; Accepted: 30 December 2024
Published online: 15 January 2025

References

1. Al-Rajhi, A. M. H. et al. Copper oxide nanoparticles as fungistat to inhibit mycotoxins and hydrolytic enzyme production by *Fusarium incarnatum* isolated from garlic biomass. *BioResources* **17**(2), 3042–3056. https://doi.org/10.15376/biores.17.2.3042-3056 (2022).
2. Al-Rajhi, A. M. H. & Abdelghany, T. M. In vitro repress of breast cancer by bio-product of edible *Pleurotus ostreatus* loaded with chitosan nanoparticles. *Appl. Biol. Chem.* **66**, 33. https://doi.org/10.1186/s13765-023-00788-0 (2023a).
3. Alsolami, A. et al. Ecofriendly fabrication of natural jojoba nanoemulsion and chitosan/jojoba nanoemulsion with studying the antimicrobial, anti-biofilm, and anti-diabetic activities in vitro. *Biomass Conv Bioref*. https://doi.org/10.1007/s13399-023-05162-0 (2023).
4. Alghonaim, M. I., Alsalamah, S. A., Ali, Y. & Abdelghany, T. M. Green mediator for selenium nanoparticles synthesis with antimicrobial activity and plant biostimulant properties under heavy metal stress. *BioResources* **19**(1), 898–916. https://doi.org/10.15376/biores.19.1.898-916 (2024).
5. Abdelghany, T. M. et al. M., and Recent Advances in Green Synthesis of Silver Nanoparticles and Their Applications: About Future Directions. A Review. *BioNanoSci* **8**(1), 5–16. https://doi.org/10.1007/s12668-017-0413-3 (2018).
6. Alsalamah, S. A., Alghonaim, M. I., Mohammad, A. M. & Abdel Ghany, T. M. Algal biomass extract as mediator for copper oxide nanoparticle synthesis: Applications in control of fungal, bacterial growth, and photocatalytic degradations of dyes. *BioResources* **18**(4), 7474–7489. https://doi.org/10.15376/biores.18.4.7474-7489 (2023).
7. Qanash, H. et al. Bioenvironmental applications of myco-created bioactive zinc oxide nanoparticle-doped selenium oxide nanoparticles,Biomass Conversion and Biorefinery2023, 1–12. (2023). https://doi.org/10.1007/s13399-023-03809-6
8. Salama, A. M. et al. Nickel Oxide nanoparticles application for enhancing Biogas Production using certain Wastewater Bacteria and aquatic macrophytes Biomass. *Waste Biomass Valor.* **12**, 2059–2070. https://doi.org/10.1007/s12649-020-01144-9 (2021).
9. Abdelghany, T. M. et al. Phytofabrication of zinc oxide nanoparticles with advanced characterization and its antioxidant, anticancer, and antimicrobial activity against pathogenic microorganisms. *Biomass Conv Bioref.* **13** (1), 417–430. https://doi.org/10.1007/s13399-022-03412-1 (2023).

10. Abdelhady, M. A., Abdelghany, T. M., Mohamed, S. H. & Abdelbary, S. A. Impact of Green Synthesized Zinc Oxide Nanoparticles for Treating Dry Rot in Potato Tubers. *BioResources* **19**(2), 2106–2119. https://doi.org/10.15376/biores.19.2.2106-2119 (2024).
11. Hoseinpour, V. & Ghaemi, N. Green synthesis of manganese nanoparticles: applications and future perspective—a review. *J. Photochem. Photobiol B Biol.* **189** (August), 234–243. https://doi.org/10.1016/j.jphotobiol.2018.10.022 (2018).
12. Al-Rajhi, A. M. H., Yahya, R. & Bakri, M. M. In situ green synthesis of Cu-doped ZnO based polymers nanocomposite with studying antimicrobial, antioxidant and anti-inflammatory activities. *Appl. Biol. Chem.* **65**, 35. https://doi.org/10.1186/s13765-022-00702-0 (2022).
13. Abdelhady, M., Abdelghany, T., Mohamed, S. & Abdelhamed, S. Biological Application of Zinc Oxide nanoparticles created by Green Method. *Egypt. J. Soil Sci.* **64** (3). https://doi.org/10.21608/EJSS.2024.272650.1731 (2024).
14. Abdelghany, T. M. et al. Green fabrication of nanocomposite doped with selenium nanoparticle-based starch and glycogen with its therapeutic activity: antimicrobial, antioxidant, and anti-inflammatory in vitro. *Biomass Convers. Biorefinery*. **13** (1), 445–445. https://doi.org/10.1007/s13399-022-03257-8 (2023).
15. EL-Moslamy, S. H. et al. Semi-industrial bio-fabrication of ZnO/MnO_2 nanocomposite using Endophytic *Streptomyces coelicolor*: characterization, Statistical Design, Exponential Pulse Fed-batch fermentation, and its antimicrobial application. *Arab. J. Sci. Eng.* https://doi.org/10.1007/s13369-024-08709-z (2024).
16. EL-Moslamy, S. H., Abd-Elhamid, A. I. & Fawal, G. E. Large-scale production of myco-fabricated ZnO/MnO nanocomposite using endophytic *Colonstachys rosea* with its antimicrobial efficacy against human pathogens. *Sci. Rep.* **14**, 935. https://doi.org/10.1038/s41598-024-51398-9 (2024b).
17. Anbumani, D. et al. Green synthesis and antimicrobial efficacy of titanium dioxide nanoparticles using *Luffa acutangula* leaf extract. *J. King Saud Univ. -Sci.* **34** (3), 101896 (2022).
18. Abdelghany, T. M. *Stachybotrys chartarum*: a novel biological agent for the extracellular synthesis of silver nanoparticles and their antimicrobial activity. *Indonesian J. Biotechnol.* **18** (2), 75–82. https://doi.org/10.22146/ijbiotech.7871 (2013).
19. Tao, C. Antimicrobial activity and toxicity of gold nanoparticles: research progress, challenges and prospects. *Lett. Appl. Microbiol.* **67** (6), 537–543. https://doi.org/10.1111/lam.13082 (2018).
20. Perachiselvi, M., Bagavathy, M. S., Samraj, J. J., Pushpalaksmi, E. & Annadurai, G. Synthesis and characterization of Mn_3O_4 nano particles for biological studies. *Appl. Ecol. Environ. Sci.* **8**, 273–277 (2020).
21. Asaikkutti, A., Bhavan, P. S., Vimala, K., Karthik, M. & Cheruparambath, P. Dietary supplementation of green synthesized manganese-oxide nanoparticles and its effect on growth performance, muscle composition and digestive enzyme activities of the giant freshwater prawn Macrobrachium rosenbergii. *J. Trace Elem. Med Biol.* **35**, 7–17 (2016).
22. Kong, J. et al. Preparation of manganese (II) oxide doped zinc oxide nanocomposites with improved antibacterial activity via ROS. *Chem. Phys. Lett.* **806**, 140053 (2022).
23. Senthilkumar, S. & Govindasamy, K. Green Synthesis of Mn-Doped ZnO nanoparticles using *Ipomoea staphylina* Leaf Extract: characterization and application of photocatalytic dye degradation, antibacterial and antioxidant activity. *ChemistrySelect* **9** (35), e202402347. https://doi.org/10.1002/slct.202402347 (2024).
24. Anantha, M. S. et al. ZnO@MnO_2 nanocomposite modifed carbon paste electrode for electrochemical detection of dopamine. *Sens. Int.* **2**, 1. https://doi.org/10.1016/j.sintl.2021.100087 (2021).
25. Du, W., Xu, X., Zhang, D., Lu, Q. & Gao, F. Green synthesis of MnO x nanostructures and studies of their supercapacitor performance. *Sci. China Chem.* **58** (4), 627–633. https://doi.org/10.1007/s11426-014-5242-4 (2015).
26. Krishnaraj, C., Ji, B. J., Harper, S. L. & Yun, S. I. L. Plant extractmediated biogenic synthesis of silver, manganese dioxide, silver doped manganese dioxide nanoparticles and their antibacterial activity against food- and water-borne pathogens. *Bioprocess. Biosyst Eng. Eng.* **39** (5), 759–772. https://doi.org/10.1007/s00449-016-1556-2 (2016).
27. Al-Rajhi, A. M., Alharbi, A. A., Alsalamah, S. A. & Abdelghany, T. M. Nanoparticles enhanced ligninolytic enzymes activity of Rotten Wood Fungus *Phanerochaete chrysosporium*. *BioResources*, **19**(2). (2024).
28. Typek, J. et al. Magnetic study of ZnMnO in ZnO/MnO nanocomposites. *IEEE Trans. Magn.* **57** (10), 234. https://doi.org/10.1109/TMAG.2021.3095729 (2021).
29. Abdelraheem, W. M., Khairy, R. M. M., Zaki, A. I. & Zaki, S. H. Effect of ZnO nanoparticles on methicillin, Vancomycin, linezolid resistance and biofilm formation in *Staphylococcus aureus* isolates. *Ann. Clin. Microbiol. Antimicrob.* **20** (1), 54. https://doi.org/10.1186/s12941-021-00459-2 (2021).
30. Faki, Y. & Er, A. Different chemical structures and physiological/pathological roles of cyclooxygenases. *Rambam Maimonides Med. J.* **12**, e0003. https://doi.org/10.5041/rmmj.10426 (2021).
31. Coulthard, G., Erb, W. & Aggarwal, V. K. Stereocontrolled organocatalytic synthesis of prostaglandin PGF2α in seven steps. *Nature* **489**, 278–281. https://doi.org/10.1038/nature11411 (2012).
32. Haque, M. F. et al. Anti-inflammatory activity of d-pinitol possibly through inhibiting COX-2 enzyme: in vivo and in silico studies. *Front. Chem.* **12**, 1366844. https://doi.org/10.3389/fchem.2024.1366844 (2024).
33. Al-Rajhi, A. M. H. et al. Antimicrobial, antidiabetic, antioxidant, and anticoagulant activities of *Cupressus sempervirensin* vitro and in silico. *Molecules* **28**(21), article 7402. https://doi.org/10.3390/molecules28217402 (2023).
34. Al-Rajhi, A. M. & Abdelghany, T. M. Nanoemulsions of some edible oils and their antimicrobial, antioxidant, and anti-hemolytic activities. *BioResources* **18**(1),1465–1481. https://doi.org/10.15376/biores.18.1.1465-1481 (2023).
35. Alghonaim, M. I., Alsalamah, S. A., Alsolami, A. & andAbdelghany, T. M. Characterization and efficiency of *Ganoderma lucidum* biomass as an antimicrobial and anticancer agent. *BioResources* **18**(4), 8037–8061. https://doi.org/10.15376/biores.18.4.8037-8061 (2023).
36. Alsalamah, S. A., Alghonaim, M. I., Jusstaniah, M. & andAbdelghany, T. M. Anti-yeasts, antioxidant and healing properties of Henna pre-treated by moist heat and molecular docking of its major constituents, chlorogenic and ellagic acids, with *Candida albicans* and *Geotrichum candidum* proteins. *Life* **13**(9), article 1839. https://doi.org/10.3390/life13091839 (2023).
37. Al-Rajhi, A. M. H. et al. Screening of Bioactive compounds from Endophytic Marine-Derived Fungi in Saudi Arabia: antimicrobial and anticancer potential. *Life* **12** (8), 1182. https://doi.org/10.3390/life12081182 (2022).
38. Abd El-Ghany, T. M. & Tayel, A. Efficacy of certain agrochemicals application at field rates on soil fungi and their ultrastructure. *Res. J. Agric. Biol. Sci.* **5** (2), 150–160 (2009).
39. Alghonaim, M. I. et al. Biosynthesis of CuO@Au NPs and its formulated into Biopolymers Carboxymethyl Cellulose and Chitosan: characterizations, antimicrobial, anticancer and antioxidant properties. *Waste Biomass Valor*. https://doi.org/10.1007/s12649-024-02469-5 (2024c).
40. Mahamuni-Badiger, P. P. et al. Biofilm formation to inhibition: role of zinc oxide-based nanoparticles. *Mater. Sci. Eng. C.* **108**, 110319 (2020).
41. Rossignol, G. et al. Involvement of a phospholipase C in the hemolytic activity of a clinical strain of *Pseudomonas fluorescens*. *BMC Microbiol.* **8**, 189 (2008).
42. Qanash, H. et al. Inhibitory potential of rutin and rutin nano-crystals against *Helicobacter pylori*, colon cancer, hemolysis and butyrylcholinesterase in vitro and in silico. *Appl. Biol. Chem.* **66**, article 79. https://doi.org/10.1186/s13765-023-00832-z (2023).
43. Alaa, A. M. et al. Synthesis, anti-inflammatory, analgesic and COX-1/2 inhibition activities of anilides based on 5,5-diphenylimidazolidine-2,4-dione scaffold: molecular docking studies. *Eur. J. Med. Chem.* **115**, 121–131. https://doi.org/10.1016/j.ejmech.2016.03.011 (2016).
44. Qanash, H. et al. Bioenvironmental applications of myco-created bioactive zinc oxide nanoparticle-doped selenium oxide nanoparticles. *Biomass Conv Bioref.* **14**, 17341–17352. https://doi.org/10.1007/s13399-023-03809-6 (2024).

45. Martínez-Vargas, B. L. et al. Synthesis and characterization of n-ZnO/p-MnO nanocomposites for the photocatalytic degradation of anthracene. *J. Photochem. Photobiol. A Chem.* **369**, 85–96. https://doi.org/10.1016/j.jphotochem.2018.10.010 (2019).
46. Hamk, M., Akcay, F. A. & Avcı, A. Green synthesis of zinc oxide nanoparticles using *Bacillus subtilis* ZBP4 and their antibacterial potential against foodborne pathogens. *Prep. Biochem. Biotechnol.* **1**, 1–10. https://doi.org/10.1080/10826068.2022.2076243 (2022).
47. Alagesan, V. & Venugopal, S. Green Synthesis of Selenium Nanoparticle using leaves Extract of *Withania somnifera* and its biological applications and photocatalytic activities. *Bionanoscience* **9**, 105–116 (2019).
48. Basak, S. et al. Phase variation of manganese oxide in the Zn@MnO nanocomposites with calcination temperature and its effect on structural and biological activities. *Sci. Rep.* **13** (1), 21542. https://doi.org/10.1038/s41598-023-48695-0 (2023).
49. El-Khawaga, A. M. et al. Correction to: green synthesized ZnO nanoparticles by *Saccharomyces cerevisiae* and their antibacterial activity and photocatalytic degradation. *Biomass Convers. Biorefinery* 1–1 (2023).
50. Gupta, M. K. et al. Synthesis of MnO_2 nanostructure and its electrochemical studies with ratio optimization of ZnO. *Ionics* **29**, 2959–2968. https://doi.org/10.1007/s11581-023-04998-w (2023).
51. Mohamed, A. A., Abu-Elghait, M., Ahmed, N. E. & Salem, S. S. Eco-friendly mycogenic synthesis of ZnO and CuO nanoparticles for in vitro antibacterial, antibiofilm, and antifungal applications. *Biol. Trace Elem. Res.* **199**, 2788–2799 (2021).
52. Elfadel, R. G. et al. Preparation of new surface coating based on modified oil-based polymers blended with ZnO and CuZnO NPs for steel protection. *Sci. Rep.* **13**, 7268 (2023).
53. Saqib, S. et al. Catalytic potential of endophytes facilitates synthesis of biometallic zinc oxide nanoparticles for agricultural application. *BioMetals* **35** (5), 967–985. https://doi.org/10.1007/s10534-022-00417-1 (2022).
54. Al Abboud, M. A. et al. Green biosynthesis of bimetallic ZnO@AuNPs with its formulation into cellulose derivative: biological and environmental applications. *Bioresour Bioprocess.* **11**, 60. https://doi.org/10.1186/s40643-024-00759-3 (2024).
55. Ogunyemi, S. O. et al. The bio-synthesis of three metal oxide nanoparticles (ZnO, MnO_2, and MgO) and their antibacterial activity against the bacterial leaf blight pathogen. *Front. Microbiol.* **11** (December), 1–14. https://doi.org/10.3389/fmicb.2020.588326 (2020).
56. Saqib, S. et al. Bimetallic assembled silver nanoparticles impregnated in *Aspergillus fumigatus* extract damage the bacterial membrane Surface and Release Cellular contents. *Coatings* **12** (10), 1505. https://doi.org/10.3390/coatings12101505 (2022).
57. Asghar, M. et al. Synthesis and characterization of microbial mediated cadmium oxide nanoparticles. *Microsc. Res. Tech.* **83** (12), 1574–1584. https://doi.org/10.1002/jemt.23553 (2020).
58. Kunkalekar, R. K., Prabhu, M. S., Naik, M. M. & Salkera, A. V. Silver-doped manganese dioxide and trioxide nanoparticles inhibit both gram positive and gram negative pathogenic bacteria. *Colloid Surf. B Biointerface*. **113**, 429–434 (2014).
59. El-Zahed, A. A., Khalifa, M. E., El-Zahed, M. M. & Baka, Z. A. Biological synthesis and characterization of antibacterial manganese oxide nanoparticles using *Bacillus subtilis* ATCC6633. *Sci. J. Damietta Fac. Sci.* **13** (3), 79–87. https://doi.org/10.21608/SJDFS.2023.242279.1136 (2023).
60. Hussain, S. et al. Tagetes erecta-mediated biosynthesis of Mn3O4 nanoparticles: Structural, Electrochemical, and Biological investigations. *ACS Omega*. **9** (33), 35408–35419 (2024).
61. Khan, H. L. A., Veeraraghavan, V. P. & Veerakumar, P. Microwave-assisted hydrothermal synthesis of Ru-doped Mn3O4 Nanoflowers for Biomedical Applications. https://doi.org/10.21522/TIJPH.2013.SE.24.01.Art005.
62. Hanif, I. et al. Coriandrum sativum mediated synthesis of Mn3O4 nanoparticles: structural and antibacterial studies. *Pol. J. Environ. Stud.* https://doi.org/10.15244/pjoes/192980 (2024).
63. Hasan, M. et al. A comparative study on green synthesis and characterization of Mn doped ZnO nanocomposite for antibacterial and photocatalytic applications. *Sci. Rep.* **14** (1), 7528. https://doi.org/10.1038/s41598-024-58393-0 (2024).
64. Anderson, M. J. et al. Alpha-toxin promotes *Staphylococcus aureus* mucosal biofilm formation. *Front. Cell. Infect. Microbiol.* **2**, 64. https://doi.org/10.3389/fcimb.2012.00064 (2012).
65. Salem, M. S. E., Mahfouz, A. Y. & Fathy, R. M. The antibacterial and antihemolytic activities assessment of zinc oxide nanoparticles synthesized using plant extracts and gamma irradiation against the uro-pathogenic multidrug resistant *Proteus vulgaris*. *Biometals* **34**, 175–196. https://doi.org/10.1007/s10534-020-00271-z (2021).
66. Ali, S. G. et al. Effect of Biosynthesized ZnO nanoparticles on Multi-drug Resistant *Pseudomonas aeruginosa*. *Antibiotics* **9** (5), 260. https://doi.org/10.3390/antibiotics9050260 (2020).
67. Mureed, S. et al. Development of multi-concentration cu:Ag Bimetallic nanoparticles as a Promising Bactericidal for antibiotic-resistant Bacteria as evaluated with Molecular Docking Study. *Nanoscale Res. Lett.* **16** (1), 91. https://doi.org/10.1186/s11671-021-03547-6 (2021). PMID: 34021844; PMCID: PMC8141091.
68. El-Sayed, A. F. et al. Synthesis, structural, molecular docking, and in vitro biological activities of Cu-doped ZnO nanomaterials. *Sci. Rep.* **14**, 9027. https://doi.org/10.1038/s41598-024-59088-2 (2024).
69. Al-Rajhi, A. M. et al. Synthesis of chitosan/Fe_2O_3/CuO-nanocomposite and their role as inhibitor for some biological disorders in vitro with molecular docking interactions studies. *Int. J. Biol. Macromol.* **280**, 135664. https://doi.org/10.1016/j.ijbiomac.2024.135664 (2024).

Acknowledgements

This work was funded by the Deanship of Graduate Studies and Scientific Research at Jouf University under grant No. DGSSR-2024-01-02066.

Author contributions

Conceptualization and writing—original draft preparation S.S., T.M.A. and M.S.A.; methodology and writing—original draft preparation, M.K.N. and M.K.T.; formal analysis and investigation, M.Y.M.E., A.A.A. and S.K.A.; All authors have read and agreed to the published version of the manuscript.

Funding

This work was funded by the Deanship of Graduate Studies and Scientific Research at Jouf University under grant no. DGSSR-2024-01-02066.

Declarations

Competing interests

The authors declare no competing interests.

Additional information

Correspondence and requests for materials should be addressed to S.S., T.M.A. or S.K.A.J.